

CRC Report No. E-55-59 1.5a

**CHARACTERIZATION OF ULTRAFINE
AND FINE PARTICULATE MATTER
EMISSIONS FROM HEAVY-DUTY
DIESEL VEHICLES**

May 2007

**Dr. Michael J. Kleeman
Michael A. Robert
Sarah G. Riddle
Chris A. Jakober**

**Department of Civil and Environmental Engineering
University of California, Davis
One Shields Avenue, Davis, CA 95616**



**COORDINATING RESEARCH COUNCIL, INC.
3650 MANSELL ROAD·SUITE 140·ALPHARETTA, GA 30022**

The Coordinating Research Council, Inc. (CRC) is a non-profit corporation supported by the petroleum and automotive equipment industries. CRC operates through the committees made up of technical experts from industry and government who voluntarily participate. The four main areas of research within CRC are: air pollution (atmospheric and engineering studies); aviation fuels, lubricants, and equipment performance, heavy-duty vehicle fuels, lubricants, and equipment performance (e.g., diesel trucks); and light-duty vehicle fuels, lubricants, and equipment performance (e.g., passenger cars). CRC's function is to provide the mechanism for joint research conducted by the two industries that will help in determining the optimum combination of petroleum products and automotive equipment. CRC's work is limited to research that is mutually beneficial to the two industries involved, and all information is available to the public.

CRC makes no warranty expressed or implied on the application of information contained in this report. In formulating and approving reports, the appropriate committee of the Coordinating Research Council, Inc. has not investigated or considered patents which may apply to the subject matter. Prospective users of the report are responsible for protecting themselves against liability for infringement of patents.

**CHARACTERIZATION OF
ULTRAFINE AND FINE
PARTICULATE MATTER EMISSIONS
FROM HEAVY-DUTY DIESEL
VEHICLES**

**FINAL REPORT TO THE COORDINATING
RESEARCH COUNCIL**

Project # E-55/59-1.5a

May 2007

**Dr. Michael J. Kleeman
Michael A. Robert
Sarah G. Riddle
Chris A. Jakober**

**Department of Civil and Environmental Engineering
University of California, Davis
One Shields Avenue, Davis, CA 95616**

Dr. Michael Hannigan

**Department of Mechanical Engineering
University of Colorado, Boulder**

DISCLAIMER

This report was prepared by the University of California at Davis as an account of work sponsored by the Coordinating Research Council (CRC). Neither the CRC, members of the CRC, the University of California at Davis nor any person acting on their behalf: (1) makes any warranty, express or implied, with respect to the use of any information, apparatus, method, or process disclosed in this report, or (2) assumes any liabilities with respect to use, or damages resulting from the use or inability to use, any information, apparatus, method, or process disclosed in this report.

ACKNOWLEDGEMENTS

This research was partially supported by the California Air Resources Board, Research Division under contract #01-306, and the National Science Foundation's Nanophases in the Environment, Agriculture, and Technology – Integrative Graduate Education, Research, and Training (NEAT-IGERT) initiative award number DGE-9972741. The authors would like to thank the staff at the WVU portable HDDV dynamometer facility in Riverside, CA for their assistance in vehicle testing. The authors would like to thank Dr. Arey and Dr. Atkinson at the University of California, Riverside for use of their laboratory space during the HDDV testing. The authors would like to thank Dr. Kimberly Prather, David Sodeman, and Stephen Toner of the University of California, San Diego for their assistance with sample collection. The authors would like to thank Dr. Jamie Schauer at the University of Wisconsin, Madison, for help with quantification standards. Finally, the authors would like to thank Dr. Nehzat Motallebi at the California Air Resources Board for help with project coordination.

TABLE OF CONTENTS

LIST OF FIGURES	v
LIST OF TABLES	vi
ABSTRACT	vii
EXECUTIVE SUMMARY	viii
Size and Composition Distribution of PM Emissions	viii
Size Distribution of Trace Organic Species.....	viii
Metals Content of Diesel Fuel, Motor Oil, and Diesel PM Emissions	ix
1.0 INTRODUCTION	1
1.1 Motivation.....	1
1.2 Research Objectives.....	2
1.3 Approach.....	2
2.0 SIZE AND COMPOSITION DISTRIBUTION OF PM EMITTED FROM HEAVY-DUTY DIESEL VEHICLES	4
2.1 Introduction.....	4
2.2 Methodology	4
2.3 Results.....	8
2.3.1 <i>Data Reduction and Quality Assurance</i>	8
2.3.2 <i>Emissions Comparisons</i>	10
2.3.3 <i>Size and Composition Distributions</i>	13
2.3.5 <i>Emissions Versus Time</i>	18
2.3.6 <i>Size Distributions Versus Driving Cycle Mode</i>	18
2.4 Conclusions.....	21
3.0 SIZE DISTRIBUTION OF TRACE ORGANIC SPECIES EMITTED FROM HEAVY-DUTY DIESEL VEHICLES	22
3.1 Introduction.....	22
3.2 Methods.....	22
3.2.1 <i>Sample Collection</i>	22
3.2.2 <i>Sample Extraction and Analysis for Organic Compounds</i>	23
3.2.3 <i>Quality Assurance</i>	25
3.3 Results and Discussion	29
3.3.1 <i>Observed Size Distribution Patterns</i>	29
3.3.2 <i>Source Profiles</i>	34
3.3.3 <i>Comparison to Previous Measurements</i>	37
3.4 Conclusions.....	41

4.0 METALS CONTENT OF DIESEL FUEL, MOTOR OIL, AND DIESEL PARTICULATE MATTER EMISSIONS.....	42
4.1 Introduction.....	42
4.2. Methodology.....	42
4.3 Results.....	43
4.3.1 ICP-MS Method Detection Limits.....	43
4.3.2 Metals Analysis of Diesel SRM 1650.....	44
4.3.3. Metals Analyses of Diesel Fuel.....	45
4.3.4 Metals Analyses of Motor Oil.....	46
4.3.5 Metals Analyses of Diesel Exhaust PM.....	47
4.4 Conclusions.....	48
5.0 CONCLUSIONS.....	49
6.0 REFERENCES.....	50

LIST OF FIGURES

Figure 1. Sample Collection System.....	5
Figure 2. Heavy Duty Diesel Vehicle (HDDV) ultrafine and fine particulate matter (PM) emissions er 56,000 lb (56k) and 66,000 lb (66k) inertial loads.....	12
Figure 3. Normalized size and composition distributions of particulate matter (PM) emitted from heavy duty diesel vehicles (HDDVs).....	14
Figure 4. Normalized ionic compound distributions of particulate matter (PM) emitted from heavy duty diesel vehicles (HDDVs).2.3.4 SMPS Scaling Factors.....	16
Figure 5. PM0.1 emissions as a function of time for different HDDVs.	19
Figure 6. Particle size distributions for HDDVs operating Particle size distributions for HDDVs operating under idle conditions (panel a) and creep conditions (panel b)..	20
Figure 7. Comparison between collocated MOUDI and RAAS filter measurements for organic compounds emitted from HDVs in the PM1.8 size fraction.....	27
Figure 8. Normalized size distribution of lubricating oil organic compounds emitted from all HDDVs examined.....	30
Figure 9. Normalized size distribution of four light PAH compounds emitted from all HDDVs examined.	31
Figure 10. Normalized size distributions for heavy PAH compounds emitted from the 1999 Freightliner operated under idle and creep conditions.	32
Figure 11. Comparison of PM 1.8 emission factors ($\mu\text{g}/\text{km}$) with those of Rogge et.al. 1993.	39
Figure 12. Comparison of PM1.8 emission factors (μg analyte / kg fuel burned) measured in the current study with those of Phuleria, et al. (2006), Zielinska, et al. (2004), Schauer, et al. (1999), and Rogge, et al. (1993).	40
Figure 13. PM0.18 emissions factors measured in the current study with and without the MOUDI after filter (AF)	41

LIST OF TABLES

Table 1. Sampling Equipment Information	6
Table 2. Heavy Duty Diesel Vehicles Tested	6
Table 3. HHDDT Driving Cycle Summary	7
Table 4. Sample Collection Summary	7
Table 5. Linear Regression Analyses for Co-located PM _{1.8} Samples	9
Table 6. HDDV Select Gas-phase and PM emission rates	13
Table 7. Instrumental Limits of Quantification and Detection	26
Table 8. Comparison of MOUDI mass to filter mass	28
Table 9. Ratio of analyte mass (µg) to organic carbon mass (g) for the PM _{1.8} size fraction.	35
Table 10. Ratio of analyte mass (µg) to organic carbon mass (g) for the PM _{0.1} size fraction.	36
Table 11. HDDV ICP-MS Methodology Summary	42
Table 12. ICP-MS Method Detection Limits	43
Table 13. ICP-MS vs. PIXE Analysis of Diesel PM SRM 1650	44
Table 14. Results from ICP-MS Diesel Fuel Metals Analyses	45
Table 15. Results from ICP-MS Diesel Motor Oil Analyses	46
Table 16. Results from ICP-MS Diesel PM Emissions Analyses	47

ABSTRACT

Ultrafine ($D_p < 100$ nm) and fine ($D_p < 1.8$ μm) particulate matter (PM) emissions from four heavy-duty diesel vehicles (HDDVs) were collected using a chassis dynamometer and dilution source sampling system. Emissions samples were collected simultaneously using cascade impactors, filter-based instrumentation, and real-time particle size distribution analyzers. The four HDDVs were tested using either partial or full California Air Resources Board (CARB) Heavy Heavy-Duty Diesel Vehicle Truck (HHDDT) driving cycles and were subjected to either 56,000 lb or 66,000 lb simulated inertial loads.

Cascade impactor and filter-based samples were subsequently analyzed for carbonaceous content, water soluble ionic species content, trace organic species, and elemental composition. Real-time measurements were scaled to size-resolved impactor reconstructed mass distributions and were then used to perform temporal analyses. This report details the sample collection methodology and laboratory analytical characterization methodologies, and presents key findings based on experimental and laboratory efforts. Ultrafine and fine PM emission rates for chemical composition speciation data are reported.

EXECUTIVE SUMMARY

Ultrafine ($D_p < 0.1 \mu\text{m}$) and fine ($D_p < 1.8 \mu\text{m}$) particulate matter (PM) emissions were collected from four Heavy Duty Diesel Vehicles (HDDVs) using a chassis dynamometer and dilution source sampling system. The four HDDVs were tested using the California Air Resources Board (CARB) Heavy Heavy Duty Diesel Test (HHDDT) driving cycle using either 56,000lb or 66,000lb simulated inertial loads. Samples were analyzed for carbonaceous content, water soluble ions, trace organic species, and elemental composition. Measurements are reported from filter samplers, cascade impactors, and scanning mobility particle sizers (SMPS).

Size and Composition Distribution of PM Emissions

Four diesel vehicles with different engine and emission control technologies were tested using the California Air Resources Board (CARB) Heavy Heavy-Duty Diesel Truck (HHDDT) 5 mode driving cycle. Vehicles were tested using a simulated inertial weight of either 56,000lbs or 66,000lbs. The exhaust particles were then analyzed for total carbon, elemental carbon (EC), organic carbon (OC), and water-soluble ions.

Ultrafine and fine PM emissions were temporally correlated and increased with vehicle age for the full 5-mode HHDDT tests. HDDV fine and ultrafine PM emission rates ranged from 181 – 581 mg/km and 25 – 72 mg/km, respectively. The majority of both ultrafine and fine PM emissions were composed of carbonaceous material. The ratio of elemental carbon (EC) to organic matter (OM) ($=1.4 \times \text{organic compounds (OC)}$) in both fine and ultrafine HDDV exhaust particles was a strong function of driving cycle. Idle and creep modes produced very low EC/OM ratios, while transient modes produced very high EC/OM ratios. The full 5-mode HHDDT tests were dominated by EC. Older diesel vehicles had higher EC/OM ratios. Calcium was the most abundant water-soluble ion with smaller amounts of magnesium, sodium, ammonium ion and sulfate also detected.

Particle mass distributions averaged over all 5-modes of the HDDV test peaked between 72 - 135 nm for vehicles of all ages. In contrast, particle mass distributions from the newest diesel vehicle had a peak diameter of ~60 nm during idle and creep driving modes while mass distributions from older vehicles had a peak at 200 nm during idle mode and 100 nm during creep mode. The newest vehicle tested was not the highest overall emitter during the overall 5-mode driving cycle, but it had the highest PM emission rate below 70 nm during the idle and creep modes of any vehicle tested.

Size Distribution of Trace Organic Species

Cascade impactor samples of diesel PM collected from four HDDVs were extracted using organic solvents and analyzed for trace organic species using GC-ITMS. Vehicles were operated under realistic driving cycles and dilution conditions were adjusted to achieve a balance between sample collection times and the need to simulate

the high dilution rates that are experienced in the atmosphere. Size distributions of PAHs, hopanes, and steranes were detected in the samples. Potential tracers for ultrafine source apportionment studies are identified and source apportionment profiles are presented for 6 vehicle tests.

17 α (H)-21 β (H)-29-norhopane, 17 α (H)-21 β (H)-hopane, $\alpha\beta\beta$ -20R-stigmastane, and $\alpha\beta\beta$ -20S-stigmastane were identified as the four most useful size-resolved PM emissions tracers. The size distribution of these compounds all peak in between 0.143-0.253 μm aerodynamic particle diameter of the idle and creep test, between 0.080-0.143 μm aerodynamic particle diameter for all 56,000 lb inertial load 5-mode tests, and in the ultrafine size fraction for the 66,000 lb inertial load 5-mode test. The ratio of ultrafine PM to total OM is highest for the 66,000 lb inertial load and lowest for the idle and creep test. No consistent trend in the percentage of OC was observed for the remaining 56,000 lb tests. All PAHs have size distributions that pass internal consistency QA/QC checks. PAHs peak between 0.080-0.143 μm aerodynamic particle diameter for the idle and creep test and between 0.080-0.143 μm aerodynamic particle diameter for all 56,000 lb tests and 66,000 lb tests.

Metals Content of Diesel Fuel, Motor Oil, and Diesel PM Emissions

The metals content of diesel fuel, motor oil, and fine PM emissions from each HDDV tested was determined using Inductively Coupled Plasma – Mass Spectrometry (ICP-MS) (7500i and 7500ce ICP-MS, Agilent Technologies, Inc., Palo Alto, CA). A method was developed using an Agilent 7500i ICP-MS to analyze the metals content of diesel fuel and motor oil; a separate method was developed using an Agilent 7500ce ICP-MS to analyze the metals content of bulk diesel PM emissions.

Used motor oil was found to contain the highest mass loading of metals, followed by the sampled tank fuel and lastly by the PM emissions. High mass loadings of 27 elements were quantified in motor oil samples from the HDDVs, and were dominated by phosphorus, sulfur, and zinc with lower concentrations of health-relevant metals such as cadmium, chromium, arsenic, strontium, and lead. Seventeen elements were detected in diesel fuel at lower concentrations than in motor oil; phosphorus, sulfur, and zinc were once again the most abundant elements detected. Up to nine metals were detected in PM emissions above MDL with potassium, calcium, and zinc present at significant concentrations. Sulfur was not observed in PM emissions; this can be attributed to low sulfur content California reformulated fuel as well as difficulty in measuring this metal using ICP-MS methodology.

Size-resolved PM emissions metals distributions were not quantified because the expected concentrations were below method detection limits. The size-resolved elemental analysis is the focus of ongoing studies.

1.0 INTRODUCTION

1.1 Motivation

Atmospheric Particulate Matter (PM) has been found to be associated with increased human mortality and morbidity in many epidemiological studies [1]. Recent studies have suggested an even stronger association between the fine fraction of PM (aerodynamic diameter $\leq 2.5 \mu\text{m}$) and morbidity/mortality [1-3]. It has been postulated that ultrafine particles (aerodynamic diameter $\leq 100 \text{ nm}$) are more pathogenic and are thus a likely candidate for some if not all observed correlation between fine PM and adverse health [4-9]. There is some evidence to support the hypothesis that ultrafine PM can localize in the mitochondria of epithelial cells where they induce major structural damage [10]. The composition and source origin of ultrafine particles must be determined to fully investigate their relationship with human health.

The characterization of particulate matter (PM) size and composition distributions emitted from in-use diesel vehicles operated under real-world conditions is essential in order to help quantify the environmental impact of these particles. Diesel PM emissions have been found to be associated with adverse health effects including increased human mortality and morbidity [2, 9, 11]. Many carcinogenic and mutagenic compounds have been measured in diesel particulate matter [12-16], and it has been designated as a Toxic Air Contaminant by the state of California [17] and as a mobile source air toxic by the U.S. Environmental Protection Agency [18]. Diesel engines are believed to be the major source of elemental carbon (EC) in both urban environments [19] and in the global atmosphere [20]. The optical properties of diesel PM have been shown to reduce regional visibility [21] as well to directly affect the radiative balance of the atmosphere [22]. In all cases, the environmental impact of the diesel exhaust particles is directly influenced by their size and composition.

Diesel engine technology and diesel fuel formulation have evolved over the past decades to reduce air pollution emissions. It is important to characterize the size and composition distribution of particles emitted from contemporary diesel engines and to compare these measurements to older engines to quantify our progress on air pollution problems. Heavy duty diesel vehicles are of special interest because these vehicles comprise only a small fraction of the total vehicles on the road but they contribute significantly to on-road mobile source primary PM emissions [23]. A common method to measure emissions from a vehicle is to operate it on a chassis dynamometer while collecting the emitted particles on filters that can then be analyzed for chemical composition. Heavy Duty Diesel Vehicles (HDDVs) with a gross vehicle weight greater than 30,000 lbs are too large to test on most chassis dynamometers under realistic driving cycles and so simplified cycles are often used. While these simplified tests provide valuable information [24-26], they do not fully reveal all the emissions trends that can occur during dynamic driving cycles. Likewise, tunnel studies [27-30] do not fully capture the range of heavy duty diesel vehicle driving cycles and direct engine dynamometer measurements [31, 32] do not fully represent emissions from complete vehicles. Attempts to measure emissions from on-road vehicles using real-time

instruments [33, 34] study the most realistic vehicle emissions, but real-time measurement techniques are still under development and so they currently provide an incomplete characterization of particle size and chemical composition. There is no perfect method to characterize emissions from heavy duty diesel vehicles, and so a combined weight of evidence approach must be continued for the present term.

1.2 Research Objectives

The purpose of this study is to report the size and composition distributions of PM released from contemporary HDDVs measured using a chassis dynamometer / dilution sampling system that employs filter-based samplers, cascade impactors, and Scanning Mobility Particle Size (SMPS) measurements. The chassis dynamometer used in this study was able to simulate realistic dynamic vehicle driving cycles and inertial loads. The data set includes a range of different vehicle types and emission control technologies. In the present study, particle size and composition distributions for fine PM_{0.1} and bulk PM_{1.8} data are reported. The composition of HDDV PM emissions are quantified as comprehensively as possible and in a manner conducive to future source apportionment modeling efforts. Vehicle emissions characteristics as a function of time for different vehicles are also presented.

1.3 Approach

The attainment of the project's research objectives was completed via efforts in three main areas. Sections 2 – 4 document the collection of the source emissions data as well as their subsequent chemical speciation and data analyses. Each section describes the relevance of the efforts described therein and draws specific conclusions based on the results generated.

Section 2 describes the sample collection phase of the project in detail and presents data on the size and composition distributions of the HDDV PM emissions. PM emissions from HDDVs were collected at the West Virginia University (WVU) portable dynamometer facility at a grocery distribution center in Riverside, CA in June and July of 2003. Four HDDVs were tested spanning a wide range in vehicle age and engine technology. Each vehicle was tested using partial or full California HHDDT driving cycles with a simulated inertial weight of either 56,000 lbs or 66,000 lbs. The exhaust from each vehicle was diluted using filtered ambient air and then collected using cascade impactors, filter-based samplers, and real-time analyzers. Particulate matter filters were then analyzed for carbonaceous and ionic species content using Total Optical Transmittance (TOT) and Ion Chromatography (IC), respectively. Test-averaged ultrafine and fine PM emission rates are reported as are reconstructed size-resolved mass distributions and temporal analyses on finer time scales.

Section 3 presents data on trace organic species present in the HDDV PM emissions. The quantification of several classes of organic compounds – namely hopanes, steranes, and Polycyclic Aromatic Hydrocarbons (PAHs) – was performed using Gas Chromatography / Mass Spectrometry (GC/MS). Ultrafine and fine emission factors of these compounds are reported and several reliable source apportionment compounds are identified.

Section 4 presents the elemental speciation of diesel fuel, motor oil, and fine PM emissions from each HDDV. Methods to measure the concentrations of up to 58 elements in these media were developed using Inductively Coupled Plasma – Mass Spectrometry (ICP-MS) instrumentation. The validity of these methods is discussed as are their Method Detection Limits (MDLs) and the resultant characterization of elemental composition.

Sections 2 – 4 collectively describe the sample collection, laboratory analyses, and chemical speciation results for ultrafine and fine HDDV PM emission samples collected in this project.

2.0 SIZE AND COMPOSITION DISTRIBUTION OF PM EMITTED FROM HEAVY-DUTY DIESEL VEHICLES

2.1 Introduction

Particulate matter emissions from heavy duty diesel vehicles (HDDVs) were collected using a chassis dynamometer / dilution sampling system that employed filter-based samplers, cascade impactors, and Scanning Mobility Particle Size (SMPS) measurements. Four diesel vehicles with different engine and emission control technologies were tested using the California Air Resources Board (CARB) Heavy Heavy-Duty Diesel Truck (HHDDT) 5 mode driving cycle. Vehicles were tested using a simulated inertial weight of either 56,000lbs or 66,000lbs. The exhaust particles were then analyzed for total carbon, elemental carbon (EC), organic matter (OM), and water-soluble ions.

HDDV fine ($\leq 1.8 \mu\text{m}$ aerodynamic diameter) and ultrafine (56 – 100 nm aerodynamic diameter) PM emission rates ranged from 181 – 581 mg/km and 25 – 72 mg/km, respectively, with the highest emission rates in both size fractions associated with the oldest vehicle tested. The ratio of EC to OM in both fine and ultrafine HDDV exhaust particles was a strong function of driving cycle and vehicle age. Older diesel vehicles produced higher EC/OM ratios than newer vehicles. Transient modes produced very high EC/OM ratios while idle and creep modes produced very low EC/OM ratios. Calcium was the most abundant water-soluble ion with smaller amounts of magnesium, sodium, ammonium ion and sulfate also detected.

The mass distribution of diesel exhaust particles measured with cascade impactors and two SMPS instruments were in good agreement in the ultrafine size range. Particle mass distributions emitted during the full 5-mode HDDV tests peaked between 100 - 180 nm and their shapes were not a function of vehicle age. In contrast, particle mass distributions emitted during the idle and creep driving modes from the newest diesel vehicle had a peak diameter of ~ 70 nm while mass distributions emitted from older vehicles had a peak diameter larger than 100 nm for both the idle and creep modes. Increasing inertial loads reduced the OM emissions, causing the residual EC emissions to shift to smaller sizes. The same HDDV tested at 56,000 lbs and 66,000 lbs had higher PM_{0.1} elemental carbon emissions (+22%) and lower PM_{0.1} OM emissions (-38%) at the higher load condition.

2.2 Methodology

PM emissions were captured from the exhaust systems of vehicles as they were driven through various driving cycles on chassis dynamometers. The emissions were diluted in two stages before sampling (Figure 1). A constant volume sampling system was used for primary exhaust dilution. The actual primary dilution rate changed as a function of time during each test. Secondary dilution was used to achieve total dilution factors that are comparable to those experienced by real-world vehicles and to avoid condensation of water in sampling lines. A constant flow rate of exhaust (after primary

dilution) was drawn into the Stack Dilution Tunnel (SDT), described by Hildemann, et al. [35] through a heated inlet line, cyclone manifold, and calibrated sample venturi. The size cut of the cyclone manifold was greater than 1.8 μm particle diameter. Secondary dilution air was passed through a pre-filter, HEPA filter, and 1.5 ft^3 of activated carbon to remove ambient PM and gas-phase organic species. Following secondary dilution and turbulent mixing in the SDT, the sample stream was aged for approximately 60 seconds in a Residence Time Chamber (RTC).

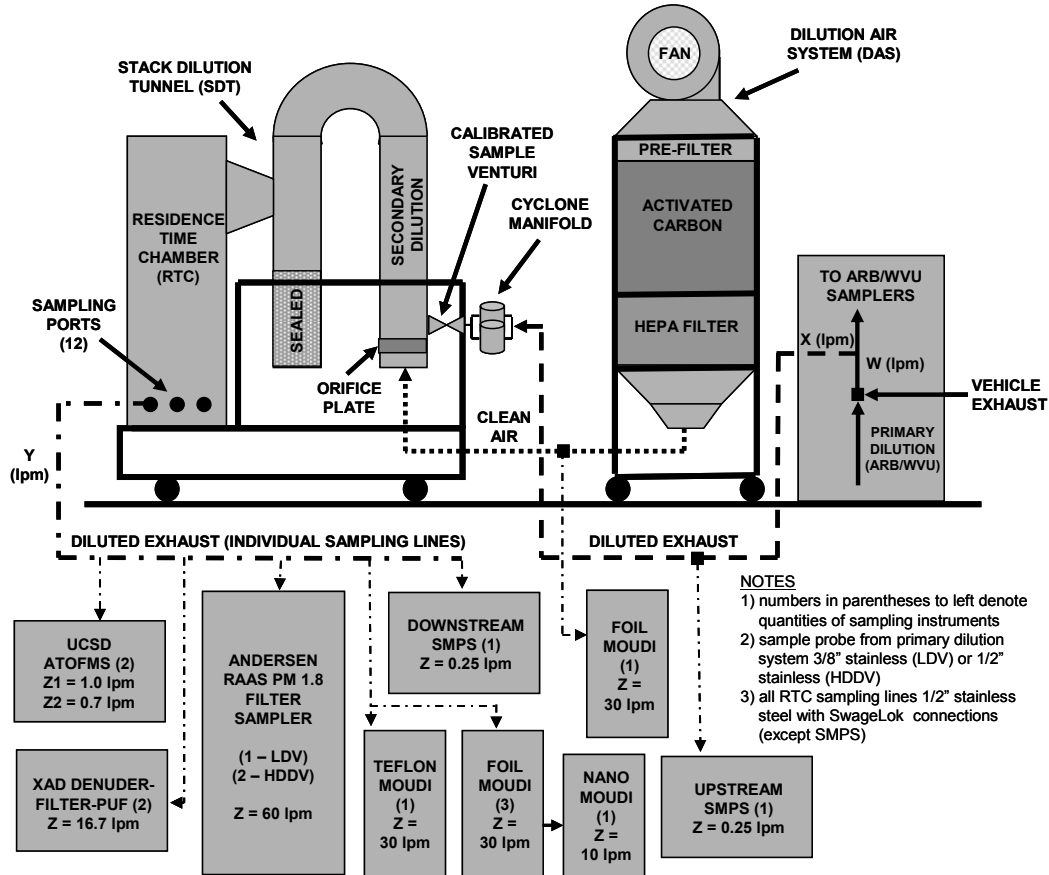


Figure 1. Sample Collection System

A variety of PM sampling equipment was employed for all chassis dynamometer tests (Table 1). Bulk $\text{PM}_{1.8}$ was collected using Andersen Reference Ambient Air Samplers (RAASs) (Andersen Instruments, Smyrna, GA). Size-resolved PM was collected using Micro Orifice Uniform Deposit Impactors (MOUDIs) (MSP Corporation, Shoreview, MN), in six size fractions between 41 nm and 1.6 μm in aerodynamic diameter. A nano-MOUDI (MSP Corporation, Shoreview, MN) was used to collect three PM size fractions below ~ 40 nm in aerodynamic diameter. Scanning Mobility Particle Sizers (SMPSs) (TSI Incorporated, Shoreview, MN) sampled time resolved PM distributions from 18 nm to 687 nm both upstream of the SDT and downstream of the RTC.

instrument	manufacturer	qty	flow rate (lpm)	lower size (µm)	upper size (µm)	collection media information		analysis type
						type	specifications	
PM _{1,8} BULK FILTER SAMPLER (RAAS)	ANDERSEN INSTRUMENTS	1 (LDGV)	60 ^a	---	1.80	QUARTZ 47mm	Pallflex 2500QAT-UP	OC/EC, trace organics
						TEFLON 47mm	Pall Teflo 2.0 um	ions, metals
		2 (HDDV)	NYLON 47mm ^b	Pall Nylasorb 1.0 um	ions			
			GLASS 47mm ^c	Pall Type A/E	ions			
MOUDI MODEL 110	MSP CORPORATION	4	30	0.41	1.60	ALUMINUM 47mm ^d	MSP Corporation	OC/EC, trace organics
		1	30	0.41	1.60	QUARTZ 37mm	Pallflex 2500QAT-UP	OC/EC
						TEFLON 47mm	Pall Teflo 2.0 um	ions, metals
						TEFLON 37mm	Pall Zeflour 2.0 um	ions, metals
NANO-MOUDI	MSP CORPORATION	1	10 ^e	0.01	0.41	ALUMINUM 47mm ^d	MSP Corporation	OC/EC, trace organics
						QUARTZ 47mm	Pallflex 2500QAT-UP	OC/EC
SMPS	TSI INCORPORATED	2	0.25	0.02	0.62	---	---	temporal PM size distributions
XAD DENUDER-FILTER-PUF ^f	UCD	2	16.7	---	1.80	Polystyrene Resin	URG-2000-30B8	trace polar organics
						QUARTZ 47mm	Pall Tissuquartz 3.0 um	
						Polyurethane Foam	URG-2000-30PC	
ATOFMS ^f	UCSD	1	1.0	0.30	2.50	---	---	single particle analyses
UF-ATOFMS ^f	UCSD	1	0.7 ^g	0.05	0.30	---	---	

^a 6 legs at 10 lpm per leg; ^b treated with sodium carbonate; ^c treated with oxalic acid; ^d baked 48 hours at 550C prior to use; ^e NANO-MOUDI instrument is downstream of a foil MOUDI and its flow rate does not contribute to the total flowrate; ^f details to be reported separately; ^g total flow rate is 28 lpm when considering upstream UCSD MOUDI

Table 1. Sampling Equipment Information

PM emissions from HDDVs were collected at the West Virginia University (WVU) transportable dynamometer facility at a grocery distribution center in Riverside, CA in June and July of 2003. Four HDDVs were tested (Table 2) spanning a wide range in vehicle age and engine technology; all vehicles tested had stock exhaust systems with no additional emissions reduction technologies installed. The chassis dynamometer used in the tests employed a combination of fly wheels and electrical motors to simulate inertial loads of either 56,000 or 66,000 pounds. All vehicles were tested using partial or full California Air Resources Board (CARB) Heavy Heavy-Duty Diesel Truck (HHDDT) cycles consisting of five modes – an idle mode, a creep mode, a transient mode, a low speed cruise, and a high speed cruise [36]. Table 3 presents details on the HHDDT driving cycle.

model year	make	mileage (miles)	load weight (lbs)	engine information				
				type	year	# cyl	disp (liters)	hp (bhp)
1999	Freightliner	138,553	56,000	Detroit Diesel Series 60	1998	6	12.7	500
1998	Kenworth	587,244	56,000	Cummins N14 460E+	1997	6	14.0	460
			66,000					
1992	Volvo	595,242	56,000	Caterpillar 3406B	1991	6	14.6	280
1985	Freightliner	988,726	56,000	Caterpillar 3406	1984	6	14.6	310

Table 2. Heavy Duty Diesel Vehicles Tested

phase / mode	avg speed	max speed	distance	time per mode
	(mph)	(mph)	(miles)	(sec)
IDLE ^a	0.0	0.0	0.00	1799
CREEP ^a	1.8	8.2	0.50	1012
TRANSIENT ^a	15.3	47.5	2.60	687
LOW-SPEED CRUISE ^a	39.9	59.3	23.00	2082
HIGH SPEED CRUISE	50.3	67.2	10.50	759

^a PHASE / MODE FOLLOWED BY 10 MINUTES WITH VEHICLE OFF

Table 3. HHDDT Driving Cycle Summary

The diesel fuel used to power HDDVs was ‘tank fuel’ (the fuel in the tank when the vehicle was procured for testing), and was assumed to be California diesel fuel. Most diesel fuels in California are alternative formulations which means that even though the nominal fuel specification calls for 10% aromatic content and no more than 500 ppm sulfur, the actual aromatic content tends to be approximately 19-20% (or higher) and the sulfur content ~150-200 ppm [37].

Table 4 summarizes the complete HDDV sample set, which consists of two background samples and six vehicle/class samples. Most HDDV samples were collected from individual vehicles driven through a full 5-mode HHDDT test; one HDDV sample was collected from a single vehicle operated under six idle and six creep modes of the HHDDT cycle. Particulate matter samples were collected after two stages of dilution. The primary dilution system mixed the hot exhaust with ambient air that was pre-filtered to remove particles. Primary dilution ratios averaged over the entire test cycle were typically 18-20 with the exception of one sample that used the idle/creep driving cycle where the primary dilution ratio was 112.5. Secondary dilution was used to increase the overall dilution factor to more realistic values. Secondary dilution ratios averaged over the entire test cycle were 5-10, yielding overall dilution rates of 129-584. Real-world dilution ratios experienced in a roadside environment in the initial period after exhaust is released to the atmosphere can reach as high as 1000. The dilution ratios used in the current test were a compromise between the desire to simulate real-world conditions and the need to collect sufficient quantities of particulate matter for chemical analysis.

sample ID	vehicle type	driving cycle	# of vehicles	# of cycles	total miles	total min	dilution ratio information		
							primary	secondary	total
HDDV-0	PRE-BLANK	n/a	n/a	n/a	n/a	187	1.0	10.0	10.0
HDDV-1	FREIGHTLINER (1999)	IDLE/CREEP	1	6	3.2	282	112.5	5.2	583.6
HDDV-2	FREIGHTLINER (1999)	56k 5-MODE	1	1	36.7	109	17.8	9.4	166.8
HDDV-3	KENWORTH (1998)	56k 5-MODE	1	1	36.6	109	17.1	7.5	128.6
HDDV-4	KENWORTH (1998)	66k 5-MODE	1	1	36.5	109	19.6	9.7	189.7
HDDV-5	VOLVO (1992)	56k 5-MODE ^a	1	1	35.8	109	18.0	9.1	163.9
HDDV-6	FREIGHTLINER (1985)	56k 5-MODE	1	1	36.1	109	19.0	8.9	169.8
HDDV-7	POST-BLANK	n/a	n/a	n/a	n/a	152	1.0	10.0	10.0

^a MAX SPEED 56-60 MPH DUE TO ENGINE GOVERNOR

Table 4. Sample Collection Summary

Dilution ratio data was used during background subtraction as part of the emissions factor calculations. Concentrations measured during tunnel blank tests were multiplied by the ratio of the (actual test primary dilution factor) / (tunnel blank primary dilution factor) and subtracted from the actual test concentration. This method assumes that the majority of the background signal is associated with the primary dilution air since measurements taken from secondary dilution air found no contamination from this portion of the sampling system. The behavior of PM size distributions below 40nm are a strong function of dilution conditions [31] and so the size distributions of PM with aerodynamic diameters smaller than 50 nm are not reported in the current study because they may not be representative of real-world conditions.

Particulate matter samples were collected using Reference Ambient Air Quality Samplers (RAAS) (Andersen Instruments, Smyrna, GA) and Micro Orifice Uniform Deposit Impactors (MOUDIs) (MSP Corporation, Shoreview MN). Sample collection media included Teflon filters (Teflo R2PJ047, Pall Corp.), quartz fiber filters (QAO47, Pall Corp.) and foil substrates (MSP Corp.). Continuous measurements of particle size distributions were made using a Scanning Mobility Particle Sizer (SMPS) (TSI Incorporated, Shoreview MN). Samples were analyzed using the methodology described by Robert, et al. [38]. Particulate matter mass was measured using a Cahn 28 microbalance. The concentration of organic and elemental carbon was measured with a Carbon Aerosol Analysis Lab Instrument (Sunset Laboratories, Tigard, OR) employing the NIOSH 5040 protocol [39] as described by Birch and Cary [40]. A multiplier of 1.4 was used to convert OC to OM [41]. Water-soluble ions were measured using an ion chromatograph (DX-600 workstation, Dionex Corporation, Sunnyvale, CA).

2.3 Results

2.3.1 Data Reduction and Quality Assurance

Protocols for sample handling and analyses are reported by Robert, et al. [38] and so only a brief summary is included here. Size-resolved PM mass distributions were constructed based on the sum of elemental carbon (EC) and organic matter (OM) measured on MOUDI stages. The maximum of three collocated MOUDI measurements in each size fraction was used to represent the most accurate size distribution data under the assumption that particle bounce was the dominant collection artifact and that particles that bounce off an upper stage will be collected by the MOUDI afterfilter [42]. Using this approach, 64% of the reconstructed MOUDI stage masses fell within the respective gravimetric data error bounds (± 1 standard deviation); 81% fell within ± 2 standard deviations.

Table 5 shows the results from a linear regression analysis between co-located $PM_{1.8}$ RAAS and summed MOUDI ($PM_{1.8}$) samples. The linear correlation coefficients for the maximum summed MOUDI mass, EC, and OM and corresponding RAAS measurements are 0.86, 0.83, and 0.80, with corresponding R^2 values ranging from 0.83 – 0.98. The agreement between collocated MOUDI and filter-based measurements is similarly strong for sodium, ammonium, magnesium, calcium, and sulfate with R^2

ranging between 0.87 – 0.97 and correlation slope ranging between 0.74 – 1.18. Reconstructed mass measurements created by summing the measured chemical species can be more accurate than gravimetric mass measurements because the uncertainty in the chemical analysis is much smaller than the uncertainty in the gravimetric measurements. The agreement between collocated MOUDI and filter-based reconstructed mass measurements is excellent with R^2 equal to 0.97 and slope equal to 0.82. The strong agreement between collocated MOUDI measurements and RAAS filter samples improves confidence in the precision of the measurements.

Sample #1	Sample #2	slope	R^2
Sum of Teflon MOUDI Gravimetric	RAAS Gravimetric	0.71	0.99
Sum of Average Foil MOUDI Gravimetric	RAAS Gravimetric	0.65	0.98
Sum of MOUDI Maxima Gravimetric	RAAS Gravimetric	0.86	0.98
Sum Average Foil MOUDI EC	RAAS EC	0.67	0.88
Sum of Maximum Foil MOUDI EC	RAAS EC	0.83	0.83
Sum of Average Foil MOUDI OM	RAAS OM	0.66	0.97
Sum of Maximum Foil MOUDI OM	RAAS OM	0.80	0.97
Sum of MOUDI Teflon Sodium	Average RAAS Sodium	1.07	0.97
Sum of MOUDI Teflon Ammonium	Average RAAS Ammonium	0.81	0.98
Sum of MOUDI Teflon Magnesium	Average RAAS Magnesium	1.18	0.87
Sum of MOUDI Teflon Calcium	Average RAAS Calcium	1.07	0.94
Sum of MOUDI Teflon Sulfate	Average RAAS Sulfate	0.74	0.97
Sum of Reconstructed MOUDI Mass	Reconstructed RAAS Mass	0.82	0.97
MOUDI Reconstructed Mass	MOUDI Gravimetric Total	1.01	0.92
RAAS Reconstructed Mass	RAAS Gravimetric	0.99	0.99

Table 5. Linear Regression Analyses for Co-located $PM_{1,8}$ Samples

The accuracy of the particle size distribution measurements made by the SMPS during this study was checked in two independent tests. Particle size distributions measured by the SMPS downstream of the secondary dilution air system were compared to upstream SMPS measurements. The ratio of the upstream and downstream measurements was approximately constant for all particles sizes above 50 nm and equal to the theoretical dilution factor calculated using measured flow rates. Furthermore, an independent set of downstream SMPS measurements was taken by Toner, et al. [36]. The average ratio of these spatially co-located (but temporally shifted) downstream SMPS measurements above 50 nm is 1.49 ± 0.20 . The offset between these SMPS measurements may have been caused by a flow rate calibration problem. The downstream SMPS used in the current study was calibrated immediately before use.

The precision of the size and composition measurements reported in the current study was evaluated by comparing the results from similar or identical tests. The idle and creep test (HDDV-1) was based on a sequence of six repetitions of the idle + creep driving modes. The average relative standard deviation of SMPS measurements across all particle sizes above 50 nm was 26% and 20% for the idle and creep modes, respectively. Tests HDDV-2-3 and HDDV-2-4 used the same vehicle driven through the

same HHDDT cycle. The only difference between the two tests is the simulated inertial load – 56,000 lbs for the former and 66,000 lbs for the latter (an 18% increase). The particle size and composition distributions measured with MOUDIs during both of these tests were similar, with the changes that did occur following a pattern that is in general agreement with the known behavior of diesel engine exhaust as a function of load. The general agreement between similar measurements increases confidence in the precision of the results.

Particle size data below 40 nm are not presented in the current study because it has been shown that PM size distributions below this size are a strong function of dilution air temperature and relative humidity [43]. These parameters were monitored but not controlled in the current study and therefore the resulting particulate data in this size range may not be representative of real-world conditions.

2.3.2 Emissions Comparisons

Figure 2 compares ultrafine and fine PM emissions from HDDVs across three categories in units of mg/km. Emissions across four HDDVs tested with full 5-mode HHDDT driving cycles and 56,000 lb inertial loads are compared in the category presented in Figure 2. Fine and ultrafine PM emissions rates for HDDVs ranged from 183 – 581 mg/km and 24 – 72 mg/km, respectively. Ultrafine and fine PM emissions rates for HDDVs were almost an order of magnitude higher than PM emissions rates for light-duty gasoline vehicles as reported by Robert, et al. [30]. When total ultrafine and fine PM emission magnitudes were normalized to the newest vehicle tested, they ranged from a factor of 0.7 to 2.9. A similar comparison between old and new gasoline-powered vehicles yielded emission rate ratios of 576 and 187 for fine and ultrafine particles, respectively (30).

Both PM_{0.1} and PM_{1.8} emissions were well correlated with vehicle production age and engine production date ($R^2 = 0.952$ and 0.960 for PM_{0.1} and PM_{1.8} in both cases and as observed by Toner, et al. (36)) but are not well correlated with vehicle/engine mileage ($R^2 = 0.508$ and 0.525 for PM_{0.1} and PM_{1.8}). These data indicate that emissions are most likely a function of engine technology and to a lesser extent engine use history.

Emissions released during an idle/creep test and a full 5-mode HHDDT test for the same vehicle with a 56,000 lb inertial load are compared in the second category presented in Figure 2. The emissions (in units of mg/km) from the idle and creep modes were much higher than those from the 5-mode HHDDT cycle because a much shorter distance was traveled during the idle and creep modes, a finding in agreement with previous studies [28, 37].

Emissions from the same vehicle tested with 56,000 and 66,000 inertial loads using the 5-mode HHDDT driving cycle are compared in the third category presented in Figure 2. Although Yanowitz, et al. [38] reported an increase in particulate carbon emissions with increasing power output for two of three HDDVs tested, there was little

difference in the PM emissions rate between 56,000 lb and 66,000 lb simulated loads in the present study; total ultrafine PM mass decreased 6% and total fine PM mass decreased 5% for the 66,000 lb test. The subtle nature of these changes relative to previous findings [38] may be due to the small increase in inertial weight (18%) or the transient driving cycles used in the current study. The speciation of the carbonaceous emissions was affected by the load condition. Ultrafine PM EC increased 22% and fine PM EC decreased 2% when load increased from 56,000 lb to 66,000 lb; ultrafine PM OM decreased 38% and fine PM OM decreased 7% when load increased from 56,000 lb to 66,000 lb. Overall, the higher load condition appears to reduce the OM emissions that coat the non-volatile EC particles, shifting the remaining EC to smaller sizes.

All of the HDDVs tested in the current study had higher ultrafine and fine PM EC emissions than PM OM emissions when tested using the full 5-mode HHDDT cycle. The average EC/OM ratio for all vehicles tested was 2.72 for ultrafine PM and 1.63 for fine PM. The EC/OM ratios were reversed for the idle and creep mode test. Average EC/OM ratios were 0.57 for ultrafine PM and 0.34 for fine PM under these driving conditions. This difference is consistent with observations by Fraser, et al. [37]. For indirect injection engines with standard fuel, Alander, et al. [39] reported PM_{2.0} EC/OM ratios between 0.64 and 1.61, with the differences attributed to changes in vehicle speed and/or power output. Ratios for indirect injection engines with reformulated fuel varied from 1.06 to 2.63, and ratios for direct injection engines with reformulated fuel ranged from 2.86 to 6.25. Numerous researchers have used the ratio of EC to OM measured in the atmosphere to estimate the amount of secondary organic aerosol formation and the contribution of diesel engines to ambient PM concentrations. The fundamental variability between EC/OM ratios generated by light-duty gasoline vehicles versus HDDVs and between HDDVs operated under different conditions illustrates the large amount of uncertainty that can enter into these types of calculations.

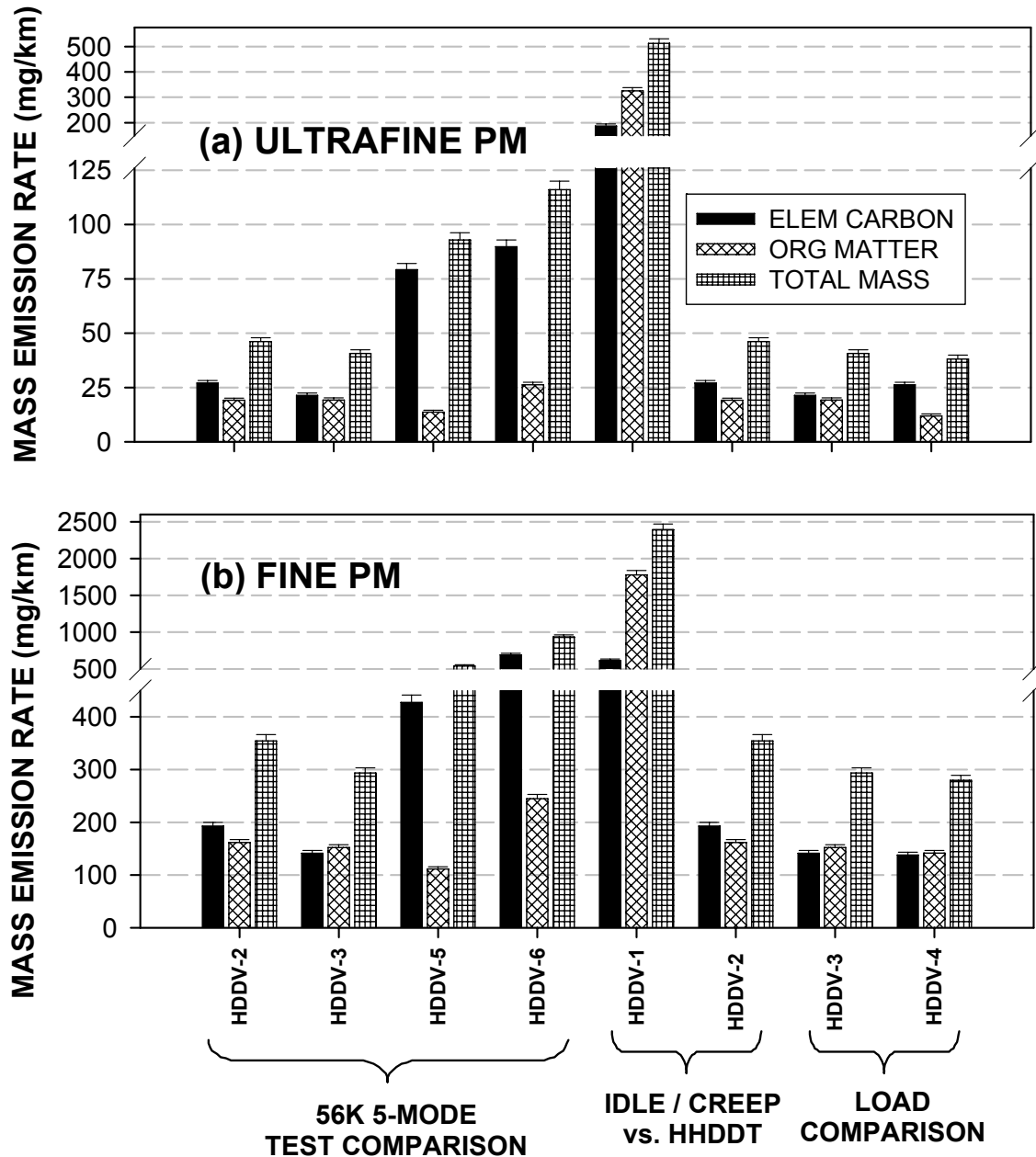


Figure 2. Heavy Duty Diesel Vehicle (HDDV) ultrafine and fine particulate matter (PM) emissions er 56,000 lb (56k) and 66,000 lb (66k) inertial loads.

Table 6 presents ultrafine PM, fine PM, EC, OM, and gaseous compound emission rates for the HDDV sample set. Whereas fine PM emission rates have been previously reported for heavy-duty gasoline vehicles, fewer studies have reported ultrafine PM emission rates and this is the first study found to specifically report ultrafine PM emission rates for heavy heavy-duty diesel vehicles operated on chassis

dynamometers using the HHDDT driving cycle. Linear regressions of PM versus gaseous species emissions in Table 6 across the vehicles tested indicate no significant correlations when the idle/creep test is excluded. However, PM emission rates are strongly correlated with each gaseous species emission rate across all samples when the idle/creep test is included.

vehicle test	Robert et al. (2005)		WVU (2004)			
	PM0.1	PM1.8	CO	CO2	NO _x	FIDHC
	(mg/km)	(mg/km)	(g/km)	(g/km)	(g/km)	(g/km)
HDDV-1	318.3	1486.2	44.6	5416	133.4	3.95
HDDV-2	28.7	220.4	4.2	1182	21.3	0.18
HDDV-3	25.3	181.4	1.5	1182	18.7	0.91
HDDV-4	28.1	172.5	1.6	1085	16.5	0.73
HDDV-5	57.7	334.9	2.1	1009	7.1	0.50
HDDV-6	72.1	580.6	4.0	1047	17.4	0.71

Table 6. HDDV Select Gas-phase and PM emission rates

Several other chassis dynamometer studies have reported fine PM emission rates comparable to those reported in Table 6. Two studies in particular have reported PM emission rates from HDDVs using the HHDDT cycle. Cocker, et al. [44] reported PM mass emission rates from a 2000 model year HDDV ranging from 81 mg/km in the cruise mode to 588 mg/km in the creep mode. Shah, et al. [36] reported an eleven-vehicle fleet (1996-2000) averaged PM emission rate ranging from 134 mg/km in the cruise mode to 635 mg/km in the creep mode. Direct comparison of these results to the results from this study is difficult due to the fact that this study reports PM mass emission rates across the entire HHDDT cycle versus each inter-cycle mode. The average fine PM emission rate in this study, excluding the idle/creep sample, is 299 mg/km. The distance-weighted average of the results reported by Cocker, et al. [44] is 164 mg/km and by Shah, et al. [36] is 257 mg/km. The idle/creep PM emission rate reported in this study is 1486 mg/km, compared to 940 mg/km by Cocker, et al. [44] and 1016 mg/km (range 479-1734 mg/km) reported by Shah, et al. [36] for the creep-only mode.

2.3.3 Size and Composition Distributions

Figure 3 shows the size and composition of PM released during six HDDV tests measured using MOUDIs and analyzed using thermal-optical EC/OC measurements as described in section 2.2. The peak in the PM mass distribution for all tests occurred between 100 - 180 nm. The full 5-mode HHDDT driving cycle tests were dominated by EC, while the idle/creep sample had a markedly larger percentage of OM emissions. This finding agrees with results reported from co-located Aerosol Time-of-Flight Mass Spectrometer (ATOFMS) measurements made by Toner, et al. [45] and it is also consistent with an independent set of diesel engine emissions measurements made by Fraser, et al. [46] where it was found that older vehicles have a higher ratio of EC/OM at all particle sizes. The 56,000 lb and 66,000 lb inertial load tests conducted with the same vehicle appeared to result in the same approximate size and composition distribution with a slight increase in ultrafine emissions at the higher loads. The EC and OM maxima in

all HDDV samples fell within 100 nm and 180 nm, which correspond to the maxima in the corresponding reconstructed mass distributions.

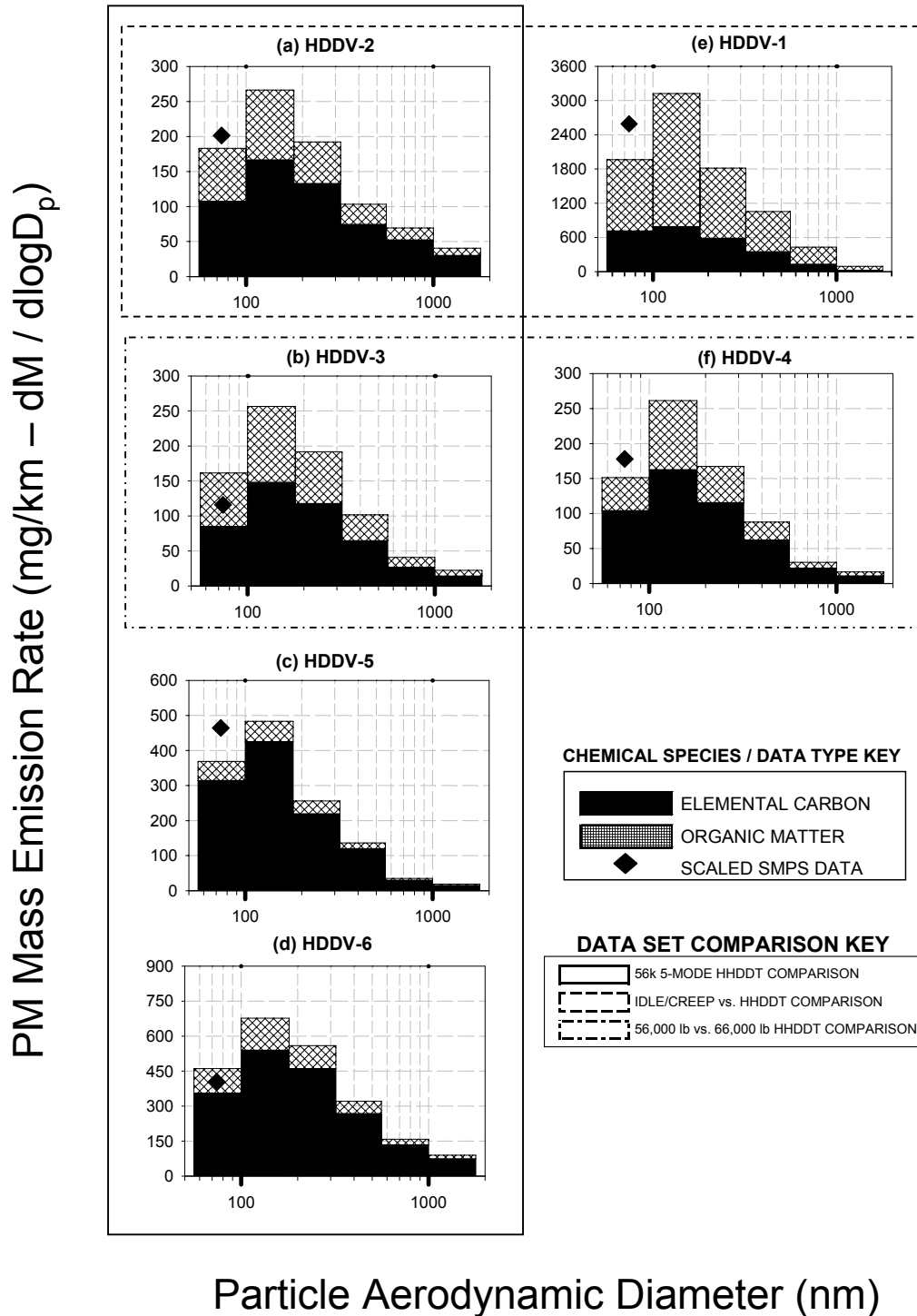


Figure 3. Normalized size and composition distributions of particulate matter (PM) emitted from heavy duty diesel vehicles (HDDVs) as measured by MOUDIs (bars) and SMPS (diamond).

Figure 4 shows the size and composition distribution of sodium, ammonium, magnesium, calcium, and sulfate released from the six HDDV samples. Error bars presented are the Method Detection Limits (MDLs) based on analytical uncertainty of the ion chromatography method utilized, defined as three times the standard deviation of seven measurements of the lowest detectable standard for each ionic species over a three-day period. The total PM_{0.1} and PM_{1.8} emissions rates are included in each panel, along with a comparison between the sum of MOUDI impactor samples and a collocated RAAS filter sample. Missing panels indicate that the measured size distribution did not pass quality control checks summarized in Section 2.3.1. Missing size distributions were typically below the IC minimum detection limits and/or did not sum to yield a PM_{1.8} concentration that was consistent with a co-located filter measurement. Due to short distance traveled during the idle/creep test, the ionic species mass emission rates (ng/km) in this sample were higher than all of the other samples. Calcium was the most abundant ion detected in the emissions. Calcium emitted from the oldest vehicles tested (HDDV-5,6) had size distributions that peaked in the ultrafine range, while calcium emitted from newer vehicles (HDDV-2,3) peaked at larger sizes. Calcium is commonly added to lubricating oil to reduce the buildup of acidity. Calcium has been observed previously in ambient ultrafine particles [42]. The ammonium size distributions also generally peaked at smaller particle sizes, but no consistent pattern was observed for the remaining ionic species distributions. Ultrafine PM emissions rates for sodium, ammonium, magnesium, calcium, and sulfate, ranged from 3 - 9 ng/km, 5 - 14 ng/km, 4 - 54 ng/km, 4 - 81 ng/km, and 1 - 8 ng/km, respectively.

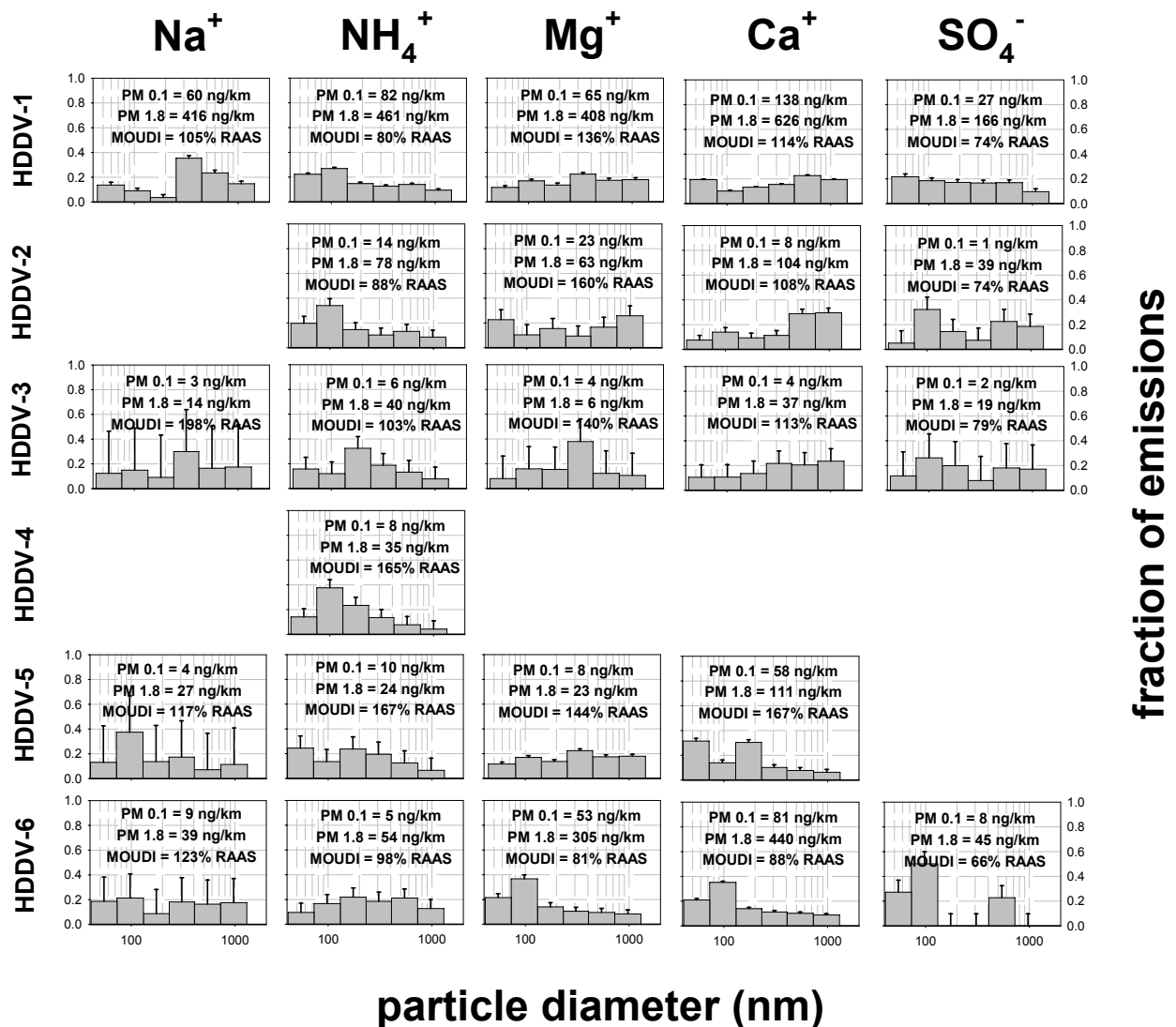


Figure 4. Normalized ionic compound distributions of particulate matter (PM) emitted from heavy duty diesel vehicles (HDDVs) as measured by MOUDIs.

2.3.4 Particle Morphology and SMPS Scaling Factors

PM material densities were estimated using the size-resolved composition information shown in Figure 2 and assuming a density of 2.0 g/cc for EC and 1.4 g/cc for organic matter [47]. Resulting average PM material densities ranged from 1.59 g/cc to 1.91 g/cc, values that bracket a recent estimate of diesel PM density of 1.78 g/cc by Park, et al. [48]. Material density was the lowest for the idle/creep sample because it was dominated by OM; the average material density excluding this test was 1.83 ± 0.06 g/cc.

Figure 3 presents scaled SMPS particle mass distributions superimposed on the reconstructed MOUDI mass distributions in the ultrafine PM range. SMPS

measurements were scaled to accurately represent the respective mass distributions because the SMPS and the MOUDI classify particle size based on differing properties [38]. Whereas the SMPS measures particle number as a function of electrical mobility diameter, the MOUDI measures particle size as a function of aerodynamic diameter.

Particle aerodynamic equivalent diameter is related to particle mobility diameter and particle effective density by the equation:

$$\rho_{\text{eff}} d_{\text{me}}^2 C_{\text{me}} = \rho_0 d_{\text{ae}}^2 C_{\text{ae}} \quad [1]$$

where d_{me} is the mobility diameter, ρ_{eff} is the PM effective density (a function of mobility diameter), ρ_0 is the unit density (1 g/cc), d_{ae} is the aerodynamic equivalent diameter, and C is the Cunningham Slip Correction Factor [49]. Effective densities for diesel PM are usually measured with particle electrical classifiers and impactors in series [31, 50-53]. Since experimental data for the effective density as a function of mobility diameter was not measured in this study (all measurements in parallel), four parameter logistic functions were fit to the effective density versus mobility diameter data measured by Park, et al. [31]. Separate curve fits were generated for an idling diesel engine and for a diesel engine under load ($R^2 = 0.994$ and 0.995 respectively) so that they could be applied correspondingly to the one idle/creep and five load samples in this study. These effective density relationships were used to iteratively solve Equation [1] to convert SMPS size cuts based on mobility diameter to aerodynamic diameter. Because the raw SMPS data assumed a material density of 1 g/cc, these same effective density relationships were also used to convert the SMPS particle volume to particle mass on a size-resolved basis. The particle effective density relationships derived from previous measurements [31] perform well in the current study for particles with diameter less than 100 nm, with the MOUDI stage 10 mass in good agreement with scaled SMPS data from 56-100 nm on a mg/km basis (slope 0.77 with $R^2 = 0.995$; slope 0.98 with $R^2 = 0.838$ excluding the idle/creep sample). The particle effective density derived in previous studies for diameters larger than 100 nm are 2 – 5 times greater than the apparent effective density of the particles measured in the current study (data not shown in Figure 3). Confidence in the MOUDI measurements from this study is enforced by the good agreement between the reconstructed summed MOUDI mass and the Andersen Reference Ambient Air Sampler (RAAS) measurements (82% as indicated in Table 5). Confidence in the SMPS data from this study is likewise enforced by agreement between SMPS measurements taken both upstream and downstream of the secondary dilution system (accounting for the effects of dilution ratio) and also the agreement between co-located SMPS measurements. The data consistency suggests that observations of low effective particle density are credible and thus an area for future investigation. The low effective particle densities observed in the current study at aerodynamic diameters above 100 nm may be caused by the multiple vehicle chassis dynamometer tests that employed transient driving cycles with dilution air at temperatures of $\sim 40^\circ\text{C}$. This contrasts with previous studies that measured effective densities in a laboratory setting with serial SMPS and impactor measurements of a single diesel engine using an engine dynamometer under steady-state conditions [31].

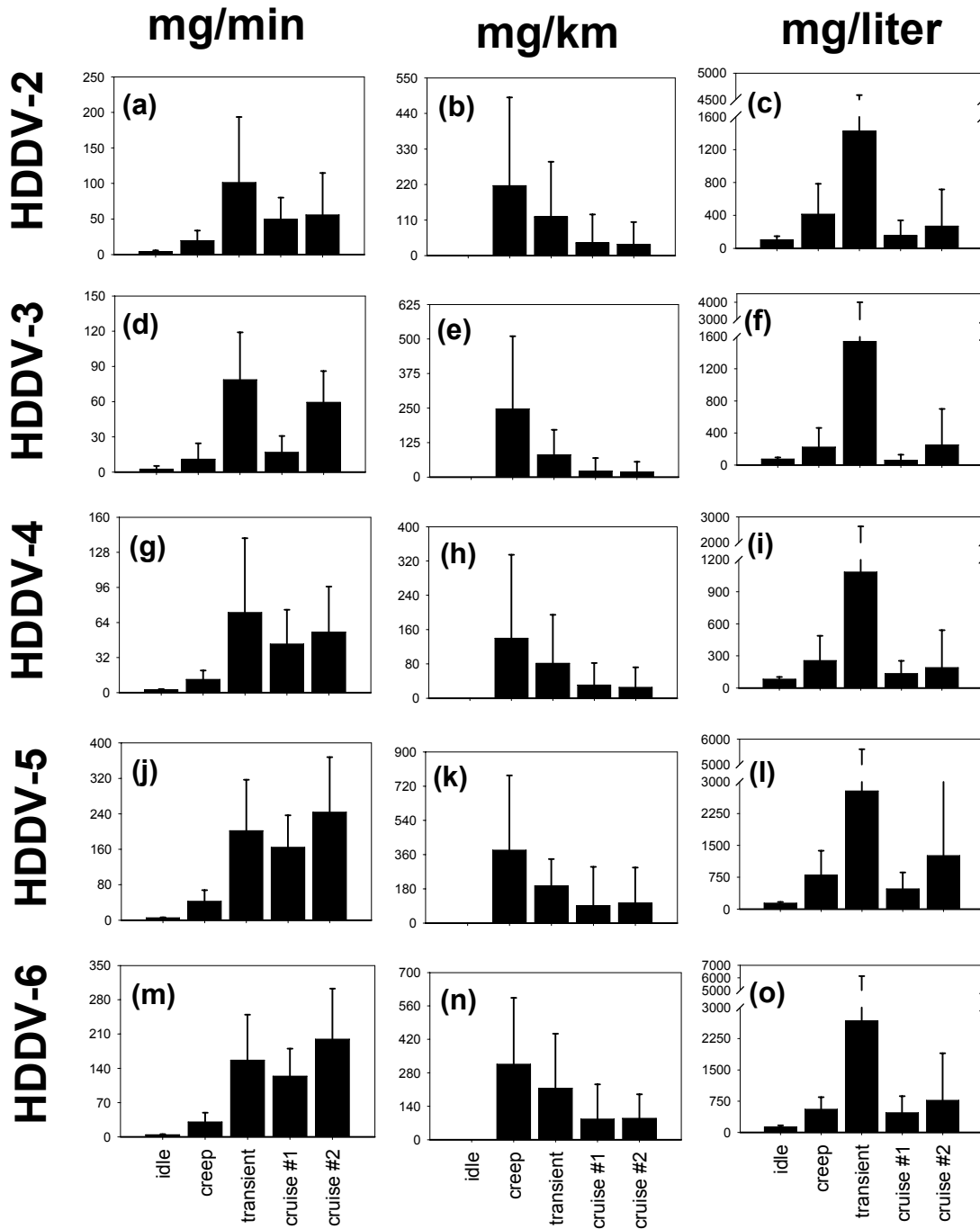
2.3.5 Emissions Versus Time

Figure 6 shows $PM_{0.1}$ emissions as a function of time (mode) for five HDDV tests using the full 5-mode HHDDT cycle in units of mg, mg/km, and mg/liter of fuel consumed. HDDV fuel consumption is calculated as the average of instantaneous (per second) CO_2 emissions data assuming 2.77 kg of gaseous CO_2 emissions per liter of diesel fuel consumed [54]. The majority of the PM mass (mg) was emitted during the transient and cruise modes. On a mass per kilometer basis, the highest emissions occurred during the creep mode, generally followed by the transient, low-speed cruise, and high-speed cruise modes (there was no data for the idle cycle as it had no associated distance traveled). On a mass per liter of fuel consumed basis, the transient mode dominated emissions in all samples. This is due to the combination of high mass emission and relatively high fuel consumption rates associated with the accelerations during the transient mode.

Uncertainty bars in Figure 6 represent one standard deviation of the magnitudes of the four individual 75 second SMPS scans that comprise the respective five minute average; each of these four data points represent the averaged cumulative mass distribution for either $PM_{0.1}$ or $PM_{0.56}$ for the vehicle tested. It follows that large error bars, such as those present in the transient and cruise modes, are indicative of highly variable mass emission rates during those driving cycle modes.

2.3.6 Size Distributions Versus Driving Cycle Mode

Figure 7 illustrates the size distribution of particle mass emissions associated with different vehicles during the idle mode (Figure 7a) and creep mode (Figure 7b), and the transient and cruise modes (Figure 7c) based on scaled SMPS data. The older vehicles generally had higher particulate matter emissions rates than the newer vehicles during these modes. The peak in the particle mass distribution for the newest vehicle occurred at approximately 70 nm during both the idle and creep modes. The peak in the particle mass distribution associated with older vehicles occurred at diameters larger than 100 nm during the idle and creep modes. Similar trends in particle size distributions were not apparent during other modes of the HHDDT tests. Toner, et al. [45] observed that the newest vehicle in this study was the highest emitter of PM on a particle number basis. Other studies of diesel emissions have observed that the vehicle with the lowest fine PM mass emissions emitted the greatest number of ultrafine particles [55, 56]. In some cases this has been attributed to changes in fuel characteristics or to engine after-treatment effects [56, 57].



HHDDT Driving Cycle Mode

Figure 5. PM0.1 emissions as a function of time for different HDDVs.

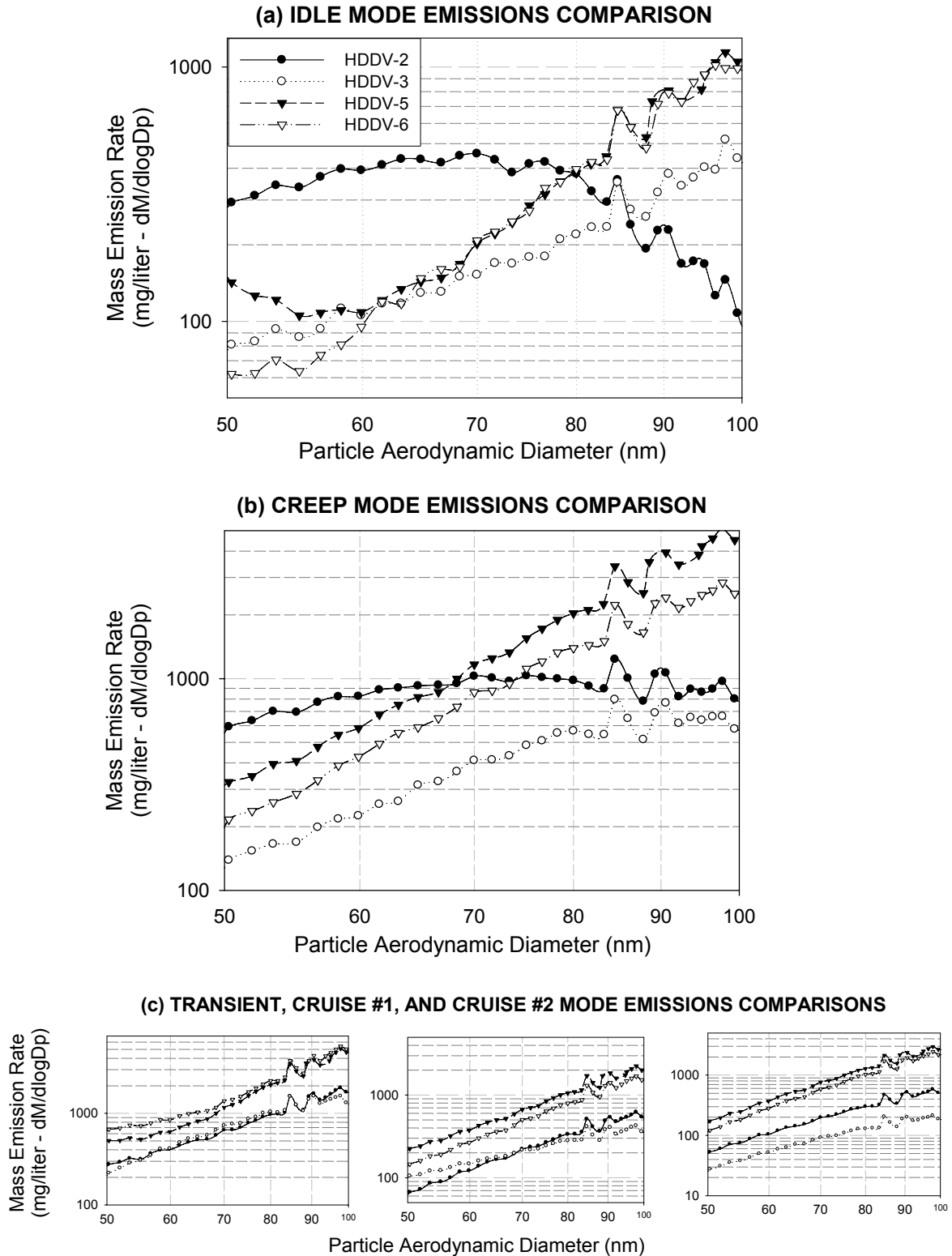


Figure 6. Particle size distributions for HDDVs operating under idle conditions (panel a), creep conditions (panel b), and transient conditions.

2.4 Conclusions

Chassis dynamometer test measurements of PM emissions from four HDDVs using the idle/creep and full HHDDT driving cycles revealed several important PM emissions trends. Ultrafine and fine PM emission rates ($\mu\text{g}/\text{km}$) increased with vehicle age as expected. The majority of the particulate matter was carbonaceous material. PM emissions using the HHDDT driving cycle were dominated by EC, with the idle/creep test was dominated by OM, results which are consistent with several other similar studies. The peak in the PM mass distributions occurred between 72 - 135 nm for all vehicles. Increasing the simulated inertial weight of the test vehicle from 56,000 lb to 66,000 lb resulted in a slight decrease for both the $\text{PM}_{0.1}$ and $\text{PM}_{1.8}$ mass emissions rates due to a reduction of OM. Fine PM EC emission rates were approximately constant at higher loads, but the EC size distribution was shifted to smaller particle diameter as the OM coating was removed. The most abundant ionic species detected was calcium with lesser amounts of magnesium, sodium ammonium ion, and sulfate.

The driving mode with the highest PM emission rates depended on the units used in the comparison. In units of mg, high PM emissions were associated with the transient and cruise modes of the HHDDT driving cycle. In units of mg/km , the highest PM emissions were observed during the creep mode. In units of mg/liter , the highest PM emissions occurred during the transient mode. The newest vehicle tested was not the highest overall emitter during the overall 5-mode driving cycle, but it had the highest PM emission rate below 70 nm during the idle and creep modes of any vehicle tested.

3.0 SIZE DISTRIBUTION OF TRACE ORGANIC SPECIES EMITTED FROM HEAVY-DUTY DIESEL VEHICLES

3.1 Introduction

Motor vehicle exhaust from diesel-powered engines is a major source of fine airborne particulate matter in urban environments [58-60]. Previous size distribution measurements of diesel vehicle exhaust aerosol indicate that these particles are at least partially in the ultrafine size range ($D_p < 100$ nm) that can penetrate deep into the lung [61, 62]. Recent evidence suggests that ultrafine particle concentrations can cause adverse health effects [2, 10, 63-65]. It is essential to determine the composition of diesel particles as a function of their size to better understand their potential health effects and to calculate their contribution to the overall ultrafine particle concentration in the atmosphere. Polycyclic aromatic hydrocarbons (PAHs), hopanes, and steranes are of particular interest when studying diesel ultrafine particles. PAHs have been shown to be both carcinogenic and mutagenic in epidemiological studies [66-68]. Hopanes and steranes can act as chemical “fingerprints” for statistical source apportionment calculations [58, 69].

Previous studies have quantified PAH, hopane, and sterane concentrations in the fine size range ($D_p < 2.5$ μm) that are emitted from medium-duty and heavy duty diesel vehicles [13, 61, 70-72] tested under a variety of load conditions. Other studies have measured the size distribution of PAHs emitted from diesel engines tested under simplified engine dynamometer tests, chassis dynamometer tests, or tunnel studies [33, 70]. No study has been published to date that describes the size-resolved emissions of PAHs, hopanes, and steranes from on-road heavy duty diesel vehicles (HDDVs) tested under realistic conditions.

The purpose of this study is to describe the size distribution of PAH, hopane, and sterane concentrations contained in airborne particles released from on-road HDDVs tested using a dilution sampling system. All vehicles were operated under realistic driving cycles and dilution conditions were adjusted to achieve a balance between sample collection times and the need to simulate the high dilution rates that are experienced in the atmosphere. Potential tracers for ultrafine source apportionment studies are identified and source apportionment profiles are presented for 6 vehicle tests.

3.2 Methods

3.2.1 Sample Collection

On-road heavy duty diesel vehicles (HDDVs) release the majority of the diesel particulate matter in urban areas within the United States. HDDVs typically have 300-600 HP engines and the loaded vehicle weight ranges from 55,000-65,000 lbs. Measuring HDDV emissions under realistic conditions poses unique challenges. Engine dynamometers can not simulate the load experienced by an engine operating in an actual

vehicle. Chassis dynamometers are generally not designed to operate at such large inertial loads. The dilution tunnels used with engine and chassis dynamometers may not completely capture the dynamics of the dilution experienced by diesel particulate matter in the real world. Tunnel studies have similar dilution artifacts and vehicles in the tunnel tend to operate at a single load condition that does not capture the full driving cycle. Chase experiments must separately quantify the diesel engine exhaust from the background aerosol. This process requires real-time instruments with relatively fast response time. Several such instruments are currently under development, but each of them requires traditional measurements to make the real-time measurements quantitative. A perfect method for the characterization of diesel engine emissions under real-world conditions does not currently exist. A weight of science approach is required using each of the techniques described above in the most realistic manner possible.

In the current study, samples of particulate matter were collected from 4 heavy duty diesel vehicles using a chassis dynamometer combined with a dilution sampling system combined with Micro Orifice Uniform Deposit Impactors (MOUDIs) (MSP Corporation, location) and Reference Ambient Air Samplers (RAAS) (Andersen Instruments, Smyrna, GA). Table 4 summarizes the 6 tests that were conducted in the present study. The basic driving cycle used for all tests was the California Air Resources Board (CARB) Heavy Heavy Duty Diesel Test (HHDDT) as summarized in Table 3. The chassis dynamometer used in these tests was one of the few such systems in the United States that is capable of testing diesel vehicles under such realistic conditions. Test # HDDV-1 focused on the first two modes (idle and creep) while all other tests used the full 5 modes of the HHDDT. Test # HDDV-4 used an inertial weight of 66,000 lbs while all other tests used an inertial weight of 56,000 lbs. The truck used in test # HDDV-5 had an engine governor that limited the maximum speed to 60 miles hr⁻¹.

Multiple legs of a RAAS sampler loaded with quartz filters were used in parallel to collect PM_{1.8} samples of diesel particulate during each of the tests described in Table 1. The sample flow rate for each filter was 10 L min⁻¹. Each filter was baked at 550 °C for 48 hrs prior to sample collection to reduce background contamination. Each filter was stored in a Petri dish lined with aluminum foil that had also been baked for 48 hrs prior to use. Petri dishes were sealed with Teflon tape and stored in a freezer at -18°C until samples were ready for analysis. Three MOUDIs loaded with aluminum foil substrates were used in parallel to collect diesel particulate matter to obtain enough mass for size-resolved GC-MS analysis. The sample flow rate through the MOUDIs was 30 L min⁻¹. Each aluminum substrate was handled with the same protocol as quartz filters described above. Aluminum substrates were weighed after sample collection to determine mass accumulation.

3.2.2 Sample Extraction and Analysis for Organic Compounds

Aluminum substrates from three MOUDI impactors were composited by size for each test and extracted as one sample. Quartz filter PM 1.8 samples were extracted individually. Sampling substrates were spiked with an isotopically labeled sterane ($\alpha\alpha\alpha$ -20R-cholestan-3 β -ol-20-one-d₄) and two isotopically labeled PAHs (chrysene-d₁₂ and

dibenz[ah]anthracene-d₁₄) then allowed to dry. Substrates were then placed into screw-cap centrifuge tubes for organic solvent extraction. Each tube is filled with ~15 mL of dichloromethane is then capped and sealed with Teflon tape. The tubes were then suspended in an ultrasonic cleaning bath and sonicated for 15 minutes. Following sonication, the tubes were centrifuged for 10 minutes at 3500 rpm to settle any suspended solids. Using baked Pasteur pipettes each extract was transferred into a graduated centrifuge tube. The sonication extraction procedure was then repeated and both the first and second extractions were combined. Extracts were then reduced in volume under Nitrogen evaporation to a final volume of 200 μL .

The organic chemical speciation data collected for this project was obtained on a Varian 3400 gas chromatograph (GC) coupled with a Varian 2000 ion-trap mass spectrometer (ITMS). The instrument was operated in electron ionization (EI) mode. This technique will be referred to as GC-ITMS from this point forward. Additionally, data files were processed using Varian Saturn GC-MS Workstation software version 5.51. with chromatographic peak integrations being performed manually.

The separation of the analytes is performed on an Agilent J&W DB-XLBMSD capillary GC column (30m x 0.25mm i.d. x 0.25 μm film thickness). The stationary phase for this particular column consists of a 5% phenyl/95% methyl substituted polysiloxane. Grade 5 helium is the carrier gas utilized for the analyses at a linear velocity of 37 cm s^{-1} . The gas was additionally purified using a VICI Helium purifier cartridge (Supelco, Bellefonte, PA)

Samples are injected using a cool-on-column technique rather than typical vapor injections. Samples volumes of 20 μL are introduced into the injection port containing a liner with an approximately 1/8" plug of glass wool. The injection port is initially at a temperature of 35 $^{\circ}\text{C}$, roughly 5 $^{\circ}\text{C}$ below the solvent boiling temperature. The initial temperature is held for 5 minutes before the injection port temperature is ramped to 300 $^{\circ}\text{C}$ at a rate of 100 $^{\circ}\text{C min}^{-1}$. The split vent remains off for the first five minutes of the injector temperature program. The introduction of samples in this manner allows us to use larger injection volumes than would be possible with a hot injector, which becomes limited by the solvent expansion volume in relation to the volume of the injection port liner.

The GC column oven is held at an initial temperature of 35 $^{\circ}\text{C}$ for the first five minutes of the analysis. This allows for cryo-focusing of the analytes on the head of the column as they vaporize out of the injection port. After five minutes the column oven is ramped to 330 $^{\circ}\text{C}$ at a rate of 5 $^{\circ}\text{C min}^{-1}$. The column is held at this temperature for ten minutes, which leads to a total analysis time of 74 minutes per injection.

Operating conditions of the mass spectrometer are as follows: The ion trap oven, manifold and transfer line are held at 250, 80 and 270 $^{\circ}\text{C}$ respectively. EI analyses are performed with an emission current of 10 μA , a target ion count of 2000 and a maximum ionization time of 25000 μsec . These operating parameters are those recommended by the manufacturer with slight modification. The GC_ITMS was operated in electron

impact (EI) ionization mass spectrometry/selected ion monitoring (SIM) mode. For PAHs the parent ion masses were scanned for. Hopanes and steranes were monitored by scanning for their predominant fragment ions, $m/z = 191$ and $m/z = 217/218$ respectively.

Multiple point calibration curves, typically 5 or 6 points, are analyzed preceding and following each set of sample extracts. These calibration solutions range in concentration from 5 to 7000 pg uL^{-1} . Calibration solutions are analyzed in order from the least to most concentrated solution to minimize any potential carryover between analyses. Following the last calibration point a solvent blank is injected to ensure no analyte carryover had occurred.

Calibration curves for the purpose of sample quantification are generated for analytes observed in the sample extracts using the instrument response for both the pre and post calibration curve. The formula utilized to generate the response curves is as follows:

$$(\text{Peak Area})_{\text{analyte}}/[\text{Conc.}]_{\text{analyte}} = \text{Response Factor} \times (\text{Peak Area})_{\text{IS}}/[\text{Conc.}]_{\text{IS}}$$

This equation can be rearranged in multiple ways to generate appropriate calibration curves for accurate analyte quantification using the internal standardization method. Chemical species were identified by a match in the relative retention time and mass spectra of the analyte compared to that of an authentic standard. When no authentic standard was available, analytes were identified by their mass spectrum and comparison of relative retention times to those in the literature. Limits of detection and limits of quantification are given in Table 7.

3.2.3 *Quality Assurance*

Figure 7 shows the agreement between collocated MOUDI and RAAS measurements for 28 organic compounds of interest in the present study. Panels (a-k) illustrate agreement for hopanes and steranes that are useful tracers for motor oil. Panels (l-bb) illustrate agreement for polycyclic aromatic hydrocarbons (PAHs) that contribute to the toxicity of diesel particulate matter. The RAAS filter masses shown in Figure 7 have been multiplied by a factor of 3 to adjust for the flow rate difference between RAAS (10 L min^{-1}) and MOUDI (30 L min^{-1}) samplers. The error bars in Figure 7 reflect the analytical uncertainty of the GC-MS analysis.

The solid line shown in each panel of Figure 7 is a linear regression analysis between the MOUDI and adjusted RAAS measurements for each organic compound. The dashed line shown in each panel of Figure 7 is a linear regression analysis between MOUDI and adjusted RAAS measurements for the average value of organic carbon measured using thermal optical carbon analysis [73]. The MOUDIs collect less organic carbon than the RAAS filter samplers because of greater volatilization losses associated with the higher flow rates in the MOUDI. The amount of organic carbon collected by the MOUDIs during the 6 HDV tests was approximately 65% of the organic carbon collected by RAAS filter samplers. The individual organic compounds shown in Figure 7 generally

have MOUDI losses that are equal or greater than the volatilization of organic carbon. Table 8 lists the regression slope and correlation coefficients for each organic compound and for the maximum and average values of organic carbon measured by MOUDI vs. RAAS filter sampler.

Compound		
<i>Hopanes</i>	LOQ (pg/ μ L) ^a	LOD (pg/ μ L) ^b
17 α (H)-21 β (H)-29-norhpane	6.2	1.8
18 α (H)-29-norneohopane ^c	6.2	1.8
17 α (H)-21 β (H)-hopane	4.8	1.4
22S-17 α (H)-21 β (H)-30 homohopane ^c	4.8	1.4
22R-17 α (H)-21 β (H)-30 homohopane ^c	4.8	1.4
<i>Steranes</i>		
20R,13 β (H)-17 α (H)-diacholestane ^c	9.7	2.9
20S,13 β (H)-17 α (H)-diacholestane ^c	9.7	2.9
$\alpha\alpha$ -20S-stigmastane ^c	5.3	1.6
$\alpha\beta$ -20R-stigmastane	5.3	1.6
$\alpha\beta$ -20S-stigmastane ^c	5.3	1.6
$\alpha\alpha$ -20R-stigmastane ^c	5.3	1.6
<i>PAHs</i>		
Phenanthrene	0.94	0.28
Anthracene	3.6	1.1
A-methylphenanthrene ^c	5.3	1.6
B-methylphenanthrene ^c	5.3	1.6
C-methylphenanthrene ^c	5.3	1.6
D-methylphenanthrene ^c	5.3	1.6
Fluoranthene	0.26	0.08
Pyrene	0.22	0.06
benzo[ghi]fluoranthene	1.0	0.30
Chrysene	0.32	0.10
benzo[b]fluoranthene	0.46	0.14
benzo[k]fluoranthene	0.44	0.12
benzo[e]pyrene	1.2	0.36
benzo[a]pyrene	0.26	0.08
indeno[1,2,3-cd]pyrene	0.62	0.18
benzo[ghi]perylene	0.76	0.22
Coronene	2.2	0.66
^a Limit of quantification determined using a signal:noise ratio of 10:1, ^b Limit of detection determined using a signal:noise ratio of 3:1, ^c no pure standard available LOQ and LOD estimated using a standard compound of the same class with the closest retention time		

Table 7. Instrumental Limits of Quantification and Detection

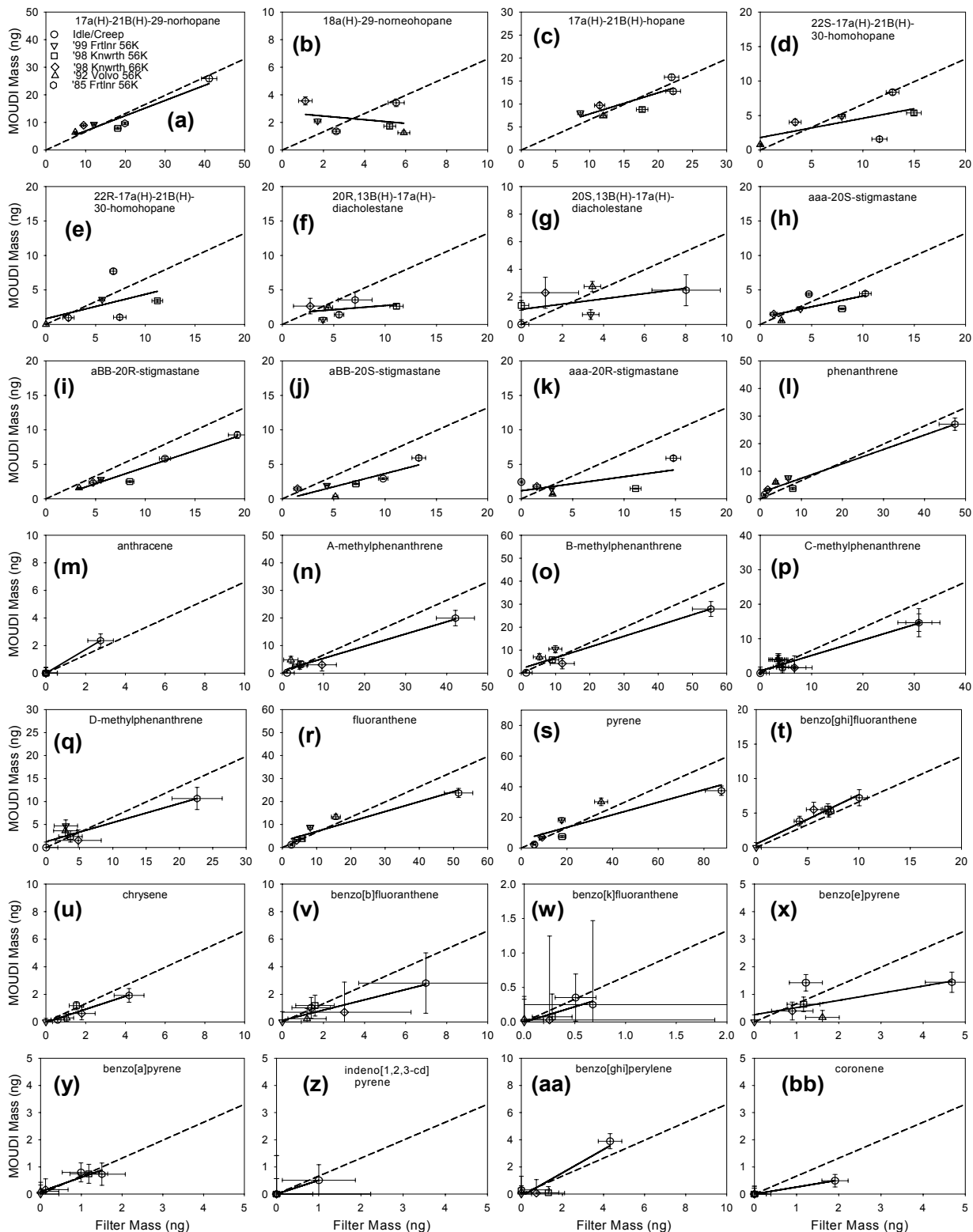


Figure 7. Comparison between collocated MOUDI and RAAS filter measurements for organic compounds emitted from HDVs in the PM_{1.8} size fraction. Uncertainty bars represent analytical uncertainty. The dashed line represents agreement between MOUDI and filter measurement.

Compound	MW	Slope	R²
Hopanes			
17 α (H)-21 β (H)-29-norhopane	398	0.5515	0.8828
18 α (H)-29-norneohopane ¹	398	-0.1328	0.2757
17 α (H)-21 β (H)-hopane	412	0.4596	0.6728
22S-17 α (H)-21 β (H)-30 homohopane ¹	426	0.2788	0.3482
22R-17 α (H)-21 β (H)-30 homohopane ¹	426	0.3541	0.2500
Steranes			
20R,13 β (H)-17 α (H)-diacholestane ¹	372	0.1188	0.1218
20S,13 β (H)-17 α (H)-diacholestane ¹	372	0.1905	0.2807
$\alpha\alpha\alpha$ -20S-stigmastane ¹	400	0.3151	0.4800
$\alpha\beta\beta$ -20R-stigmastane	400	0.4809	0.9487
$\alpha\beta\beta$ -20S-stigmastane ¹	400	0.3830	0.7113
$\alpha\alpha\alpha$ -20R-stigmastane ¹	400	0.2034	0.4294
PAHs			
Phenanthrene	178	0.5528	0.9657
Anthracene	178	0.8578	1.0000
A-methylphenanthrene	192	0.4424	0.9396
B-methylphenanthrene	192	0.4685	0.9173
C-methylphenanthrene	192	0.4471	0.9602
D-methylphenanthrene	192	0.4512	0.9169
Fluoranthene	202	0.4325	0.9060
Pyrene	202	0.4094	0.8844
benzo[ghi]fluoranthene	226	0.7132	0.9435
Chrysene	228	0.4732	0.8796
benzo[b]fluoranthene	252	0.3729	0.8403
benzo[k]fluoranthene	252	0.4466	0.7125
benzo[e]pyrene	252	0.2600	0.4450
benzo[a]pyrene	252	0.5261	0.9033
indeno[1,2,3-cd]pyrene	276	0.5082	1.000
benzo[ghi]perylene	276	0.8596	0.8831
Coronene	300	0.2577	1.000
Organic Carbon			
organic carbon (average)		0.6609	0.9715
organic carbon (maximum)		0.7804	0.9740

Table 8. Comparison of MOUDI mass to filter mass

Consistency between MOUDI and filter measurements is a necessary check to build confidence in the accuracy of the size distribution measurements. Hopanes 17 α (H)-21 β (H)-29-norhopane (Figure 8 a) and 17 α (H)-21 β (H)-hopane (Figure 8 c) appear to exhibit the most consistent behavior between MOUDI and filter measurements as demonstrated by correlation slopes = 0.5515-0.4596 and correlation coefficients R² = 0.8828- 0.6728. Likewise, steranes $\alpha\beta\beta$ -20R-stigmastane (panel i) and $\alpha\beta\beta$ -20S-stigmastane (panel j) exhibit the most consistent behavior between MOUDI and filter measurements with correlation slopes = 0.4809 - 0.3830 and correlation coefficients R² = 0.9487- 0.7113. These four species appear to have the greatest promise as size-resolved tracers for diesel particulate matter. The majority of the PAH species appear to behave consistently when collected with MOUDI and filter samplers although some species are present at concentrations that are below the analytical uncertainty.

3.3 Results and Discussion

3.3.1 Observed Size Distribution Patterns

Size distributions for lubricating oil tracers and PAHs are presented in Figures 8 and 9 respectively. The solid line represents the measured value normalized to total analyte mass while the dashed lines illustrate the analytical uncertainty (sample collection uncertainty is not shown). Figure 8 Row 1 shows the normalized size distribution of lubricating oil tracer compounds emitted from a 1999 Freightliner HDDV operated using the idle and creep portions of the HHDDT. All of the hopanes emitted during the idle and creep modes had a mass distribution peak between 0.18-0.32 μm aerodynamic particle diameter. The size distributions of the two most promising tracer hopanes are consistent with the size distribution of one of the promising tracer steranes ($\alpha\beta\beta$ -20R-stigmastane). The size distribution of the other promising tracer sterane ($\alpha\beta\beta$ -20S-stigmastane) is discontinuous with zero mass detected between 0.18-0.32 μm aerodynamic particle diameter. Based on these size distributions 15-20% of the most suitable tracer mass appears to be contained in the smallest size fraction (0.056 – 0.10 μm aerodynamic particle diameter) during idle and creep operation.

Figure 8 Row 2 shows the normalized size distribution of hopanes and steranes emitted from a 1999 Freightliner HDDV operated using the full 5-mode HHDDT with a simulated inertial weight of 56,000 lbs. A comparison of Row 9 and Row 2 illustrates the behavior of the same vehicle operated under idle+creep modes vs. the full 5-mode HHDDT cycle. The hopanes emitted during the HHDDT have a normalized size distribution that peaks between 0.10-0.18 μm aerodynamic particle diameter as do the size distributions for the two primary steranes measured. Based on the results shown in Figure 8 Row 2, the fraction of the tracer mass contained in particles with aerodynamic diameter between 0.056-0.10 μm is approximately 25-30%.

Figure 8 Row 3 shows that the normalized hopane size distribution emitted by the 1998 Kenworth HDDV operated using the full 5-mode HHDDT with an inertial weight of 56,000 lbs peaks between 0.10-0.18 μm aerodynamic particle diameter. The two most promising steranes exhibit a peak in their normalized size distributions similar to the hopanes. The fraction of the tracer mass contained in particles with aerodynamic diameter between 0.056-0.10 μm is approximately 10-30% of the total tracer mass collected.

Figure 8 Row 4 presents the size distributions for the hopanes and steranes for the 1998 Kenworth HDDV operated using the full 5-mode HHDDT with an inertial weight of 66,000 lbs. A comparison of Row 3 and Row 4 illustrates the behavior of the same vehicles tested using the 5-mode HHDDT using different inertial weights. Shifts to smaller sizes are observed for the hopanes and steranes under higher loads. The peak in the normalized size distribution of the lubricating oil tracers occurs in the ultrafine size fraction, 0.056 – 0.01 μm aerodynamic particle diameter, under a simulated inertial load of 66,000 lbs. The increased load produced approximately twice as much tracer mass (20-45%) in the ultrafine size fraction (see Figure 8 Row 3 vs. Row 4).

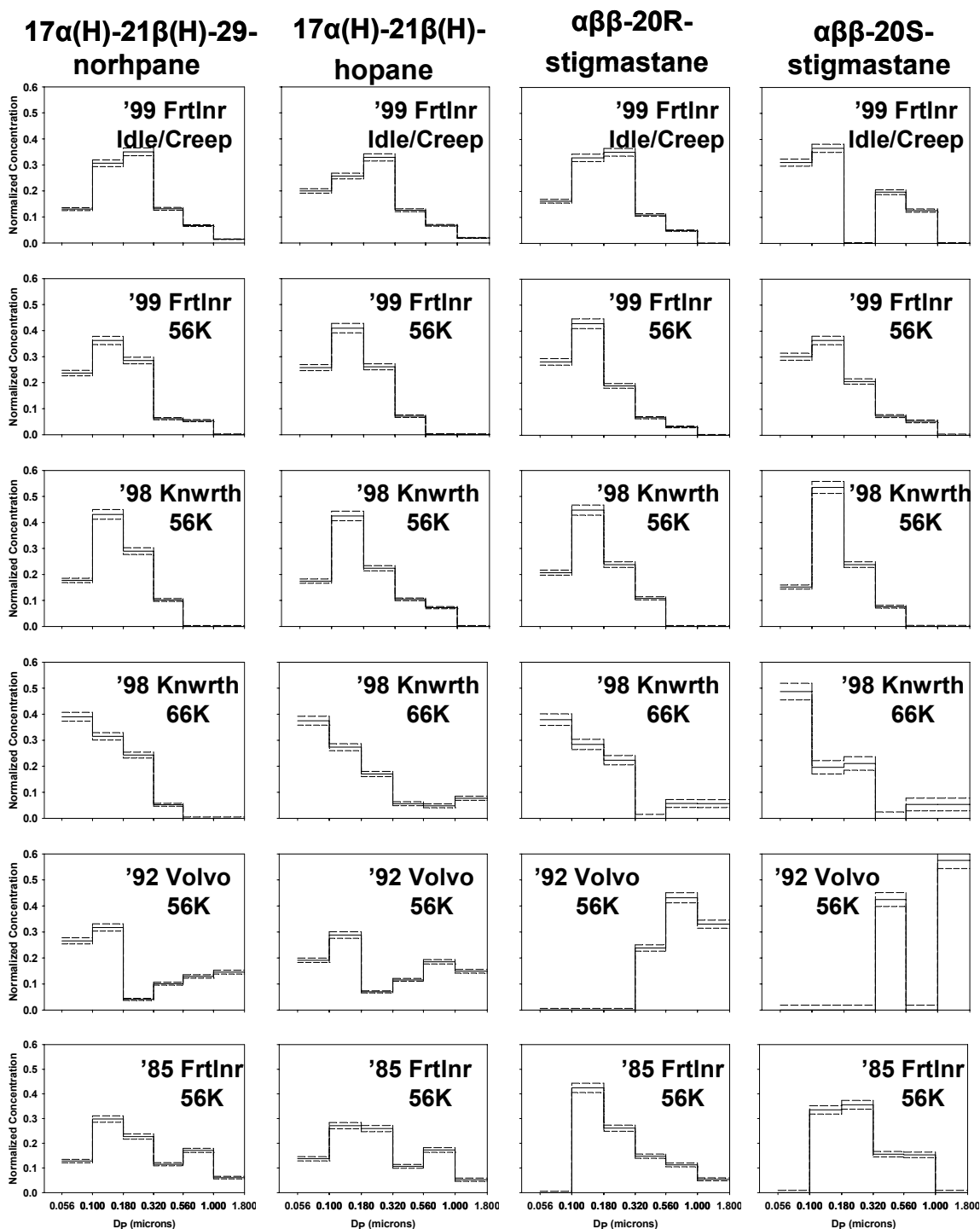


Figure 8. Normalized size distribution of lubricating oil organic compounds emitted from all HDDVs examined. Size distributions were normalized to total analyte mass for each analyte observed on the MOUDI substrates. The solid line represents the measured value while the dashed lines illustrate the analytical uncertainty.

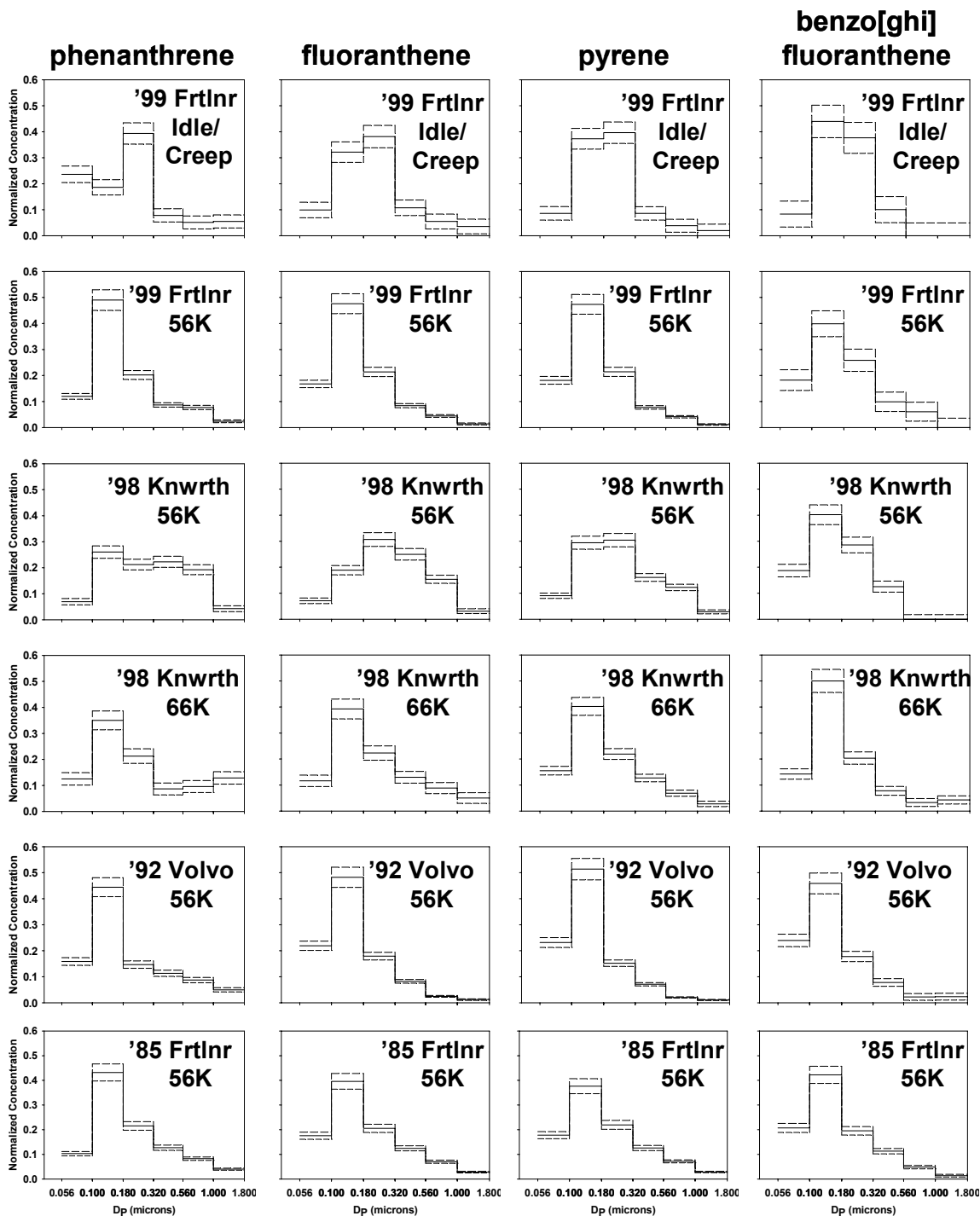


Figure 9. Normalized size distribution of four light PAH compounds emitted from all HDDVs examined. Size distributions were normalized to total analyte mass for each analyte observed on the MOUDI substrates. The solid line represents the measured value while the dashed lines illustrate the analytical uncertainty.

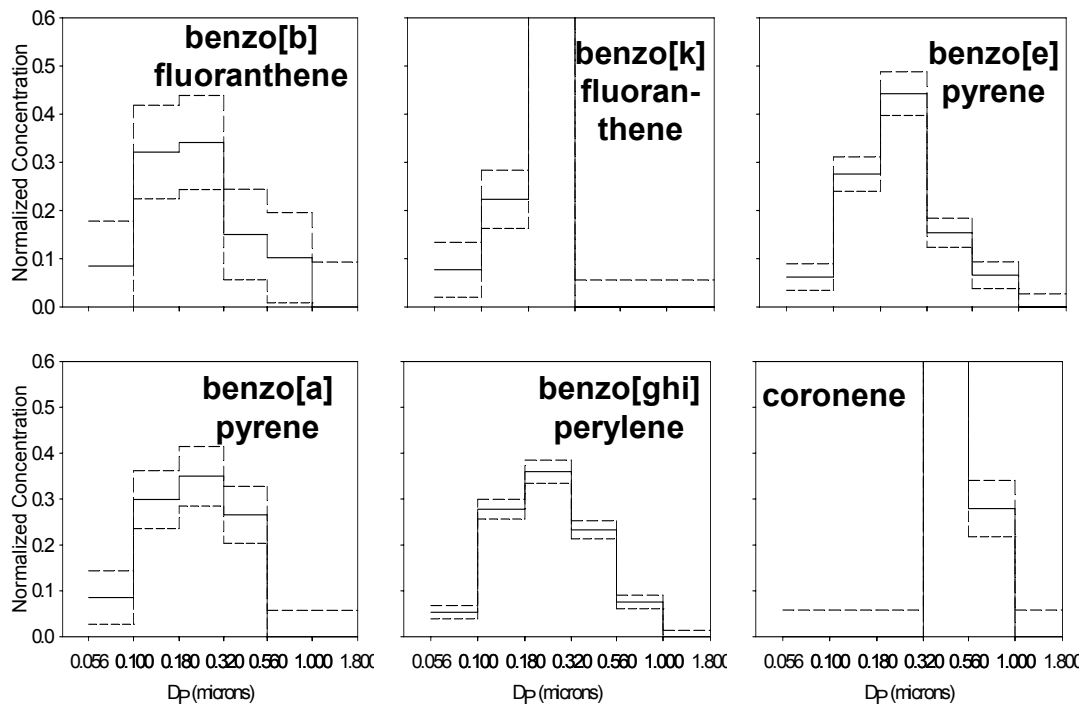


Figure 10. Normalized size distributions for heavy PAH compounds emitted from the 1999 Freightliner operated under idle and creep conditions. Size distributions were normalized to total analyte mass for each analyte observed on the MOUDI substrates. The solid line represents the measured value while the dashed lines illustrate the analytical uncertainty.

Trends in size distributions for the 1992 Volvo HDDV operated using the full 5-mode HHDDT with an inertial weight of 56,000 pounds are shown in Figure 8 Row 5. Size distributions were obtained for both hopanes. The peak in the distribution for these analytes occurred between 0.10-0.18 μm aerodynamic particle diameter with varying amounts in the other size fractions. Discontinuous size distributions were observed for both steranes. No other analytes in any sample exhibited this normalized size distribution pattern and the reason for the variation in this sample is unknown.

Normalized size distributions for trace organic species emitted from the 1985 Freightliner HDDV operated using the full 5-mode HHDDT with an inertial weight of 56,000 lbs are shown in Figure 8 Row 6. Lubricating oil tracers identified in this test had size distributions that peaked between 0.10 – 0.18 μm aerodynamic particle diameter, with a second smaller mode observed for hopanes between 0.56-1.0 μm aerodynamic particle diameter. Approximately 10 - 20 % of the observed tracer mass is contained in particles between 0.056-0.10 μm is aerodynamic diameter.

Rows 1-4 of Figure 8 generally illustrates that increasing load causes the size distribution of the trace compounds emitted from HDDVs produced after 1998 to decrease from ~ 0.32 μm aerodynamic diameter to < 0.10 μm aerodynamic diameter. Rows 5 and 6 of Figure 8 generally illustrate that the size distribution of tracer

compounds emitted from older technology vehicles becomes more bimodal. This latter trend may be related to the control technology or it may be caused by the general wear on the older vehicles. The construction of fleet-average emissions factors for tracer compounds in different size fractions will need to consider vehicle age and driving mode in order to accurately represent the emissions profiles.

Figure 9 illustrates the normalized size distributions of light 3 and 4 ring polycyclic aromatic hydrocarbons (PAHs) emitted from HDDVs in a format that is analogous to Figure 8. The first row of Figure 9 shows that light PAHs emitted from a 1999 Freightliner HDDV operated using the idle and creep portions of the HHDDT peaked between 0.10-0.32 μm aerodynamic particle diameter. Rows 2-6 of Figure 9 illustrate that PAH emissions from all 5-mode HHDDT driving cycle test peaked between 0.10-0.18 μm aerodynamic particle diameter. The only exception to this trend was that size distributions of light PAHs emitted from the 1998 Kenworth HDDV were somewhat variable (Figure 9 Row 3). Four ring PAHs fluoranthene and pyrene exhibited a peak in their normalized size distribution between 0.18 – 0.56 μm aerodynamic particle diameter, but also had a significant portion of their mass between 0.10-0.18 μm aerodynamic particle diameter. Benzo[ghi]fluoranthene emitted from the 1998 Kenworth HDDV peaked between 0.18 – 0.56 μm aerodynamic particle diameter.

The mix of PAHs emitted from HDDVs in the current study was sensitive to vehicle load conditions and control technology. Figure 10 shows the size distribution of five and six ring nonvolatile PAHs including benzo[b]fluoranthene, benzo[k]fluoranthene, benzo[e]pyrene, benzo[a]pyrene, benzo[ghi]perylene, and coronene that were detected in the idle and creep emissions. These larger PAHs were detected in much smaller amounts in the other driving cycles thus discontinuous size distributions were observed. These heavy PAH compounds exhibit the same general size distribution pattern as the hopanes and the light PAHs with the exception of coronene (Figure 10 Row 2) which was only observed in particles larger than 0.32 μm aerodynamic particle diameter. Coronene has been identified as a potential tracer for gasoline-powered vehicles [58, 74]. The presence of coronene in the exhaust of diesel engines operated under idle and creep conditions suggests that this compound is not a unique tracer for gasoline engine exhaust. The oldest vehicle tested (1985) had much higher emissions of PAHs than any other vehicle considered in the present study. Anthracene (not shown) was detected in the emissions from the 1985 vehicle with a slightly higher concentration in the ultrafine size fraction.

3.3.2 Source Profiles

Ratios of analyte mass (μg) to total organic carbon mass (g) for the PM 1.8 and the PM 0.1 size fractions are shown in Tables 9 and 10 respectively. Total organic and elemental carbon was measured from a subsection of each sample using a thermal-optical measurement technique as discussed in Section 2. The relative analyte/OC concentrations can be used as source profiles to calculate contributions to particulate matter mass in the PM1.8 and PM0.1 size fractions. A comparison of Tables 9 and 10 reveals several important trends. The relative abundance of the motor oil tracers in both the fine and ultrafine size fractions is a function of load condition. Columns 2 and 4 in Tables 9 and 10 compare the relative abundance of tracers emitted from the same vehicle tested under idle+creep and HDDT driving cycles with an inertial weight of 56,000 lbs. Columns 6 and 8 of Tables 9 and 10 compare the relative abundance of tracers emitted from the same vehicle tested under the HDDT driving cycle with an inertial weight of 56,000 lbs and 66,000 lbs. In both cases, the increased load condition results in a reduction of the tracer mass in the PM1.8 size fraction and an increase in the tracer mass in the PM0.1 size fraction. The decrease of hopanes and steranes in the fine particle fraction at higher loads matches trends observed in previous studies [75]. Part of this reduction may be related to increased combustion temperatures at higher loads causing thermal destruction of the tracers. Higher engine loads also decrease the effective density of the diesel exhaust particles [31] causing a greater fraction of the residual tracers to shift to the ultrafine size range collected by the MOUDIs.

A comparison of columns 4, 6, 9, and 11 in Table 9 and 10 illustrates that the relative abundance of motor oil tracers in the PM1.8 and PM0.1 size fractions is not a strong function of vehicle age when the vehicles were tested with the HHDDT and 56,000 lbs inertial weight. Steranes were generally not detected in the two oldest vehicles that were tested (1992 and 1985). Steranes in the ultrafine size range were generally not detected in the two oldest vehicles that were tested (1992 and 1985). Hopane and sterane emissions increase with the oil consumption rate (related to vehicle age and maintenance) and decrease with higher engine load (exhaust temperature) [31]. In the present study, the oldest vehicle (1985) had the highest emission rates of hopanes and steranes during the basecase 56,000lb HHDDT test. The second oldest vehicle (1992) also had the lowest rated engine horsepower, putting it under higher relative load during the basecase test. As a result, the second oldest vehicle had the lowest emissions rates of hopanes and steranes in the current study.

The relative abundances of PAHs in the PM0.1 and PM1.8 size fractions emitted from the oldest vehicle tested (1985 HDV) were significantly higher than for any other vehicle tested. Tests with greater loads generally produced emissions with a greater relative abundance of light PAHs but with reduced concentrations of heavy PAHs. Some heavy PAHs were only observed during the idle and creep test.

Compound	1999 Frtlnr Idle/Creep		1999 Frtlnr 56K		1998 Knwrth 56K		1998 Knwrth 66K		1992 Volvo 56K		1985 Frtlnr 56K	
	ratio	error	ratio	error	ratio	error	ratio	error	ratio	error	ratio	error
<i>Hopanes</i>												
17 α (H)-21 β (H)-29-norhpane	348.4	34.4	171.5	17.0	285.0	32.7	163.1	19.7	144.9	18.5	177.0	16.0
17 α (H)-21 β (H)-hopane	186.2	18.4	122.3	12.2	278.5	31.9	196.6	24.7	234.3	29.7	197.7	18.2
<i>Steranes</i>												
$\alpha\beta\beta$ -20R-stigmastane	101.7	10.1	78.5	7.8	133.3	15.3	81.7	11.3	65.2	8.3	171.8	15.7
$\alpha\beta\beta$ -20S-stigmastane ¹	83.3	8.2	61.5	6.1	112.9	13.0	25.3	6.7	101.1	12.8	118.4	11.1
<i>PAHs</i>												
phenanthrene	9.2	2.9	96.6	12.5	125.1	18.0	31.4	9.3	73.8	12.4	422.7	47.8
anthracene	ND		ND		ND		ND		ND		24.5	6.0
A-methylphenanthrene	9.7	14.9	60.0	25.7	70.5	29.1	165.8	62.5	40.6	34.7	375.6	50.8
B-methylphenanthrene	12.1	14.9	141.0	29.7	142.8	33.5	205.4	64.5	103.2	37.1	493.8	61.9
C-methylphenanthrene	ND		51.6	25.5	68.2	29.0	114.5	60.6	66.9	35.4	275.5	42.4
D-methylphenanthrene	ND		41.8	25.2	57.5	28.6	82.8	59.8	56.3	35.1	201.9	37.2
fluoranthene	22.3	3.7	115.6	14.5	91.5	13.4	71.6	13.1	305.9	44.3	458.9	51.8
pyrene	48.1	7.2	250.8	30.8	282.1	39.5	156.9	24.3	684.8	98.6	781.5	88.0
benzo[ghi]fluoranthene	13.1	2.7	15.5	4.1	56.2	8.8	41.8	7.3	79.5	12.6	106.0	12.3
chrysene	5.0	2.9	ND		24.2	6.3	30.9	12.1	20.5	7.2	37.3	7.3
benzo[b]fluoranthene	11.9	8.0	ND		25.1	15.0	51.9	56.1	23.5	18.5	62.3	29.6
benzo[k]fluoranthene	4.3	1.7	ND		4.4	3.1	4.3	28.0	ND		6.0	14.6
benzo[e]pyrene	10.4	3.4	ND		18.4	6.5	15.4	8.6	31.6	8.7	41.8	6.5
benzo[a]pyrene	8.4	4.0	ND		18.7	7.6	2.1	9.5	ND		13.4	5.2
indeno[1,2,3-cd]pyrene	8.5	7.4	ND		ND		ND		ND		ND	
benzo[ghi]perylene	36.7	5.8	ND		20.7	8.3	12.6	23.6	ND		ND	
coronene	16.2	3.0	ND		ND		ND		ND		ND	

¹ Analyte identification based on comparisons to relative retention times to those in the literature.
² ND = not detected

Table 9. Ratio of analyte mass (μg) to organic carbon mass (g) for the RAAS filter measurements for organic compounds emitted from HDDVs in the PM1.8 size fraction. Uncertainty values represent analytical uncertainty.

Compound	Frtlnr Idle/Creep		Frtlnr 56K		Knrwth 56K		Knrwth 66K		Volvo 56K		Frtlnr 56K	
	ratio	error	ratio	error	ratio	error	ratio	error	ratio	error	ratio	error
<i>Hopananes</i>												
17 α (H)-21 β (H)-29-norhpane	149.6	9.0	138.9	9.0	104.6	6.7	560.4	48.7	189.6	14.1	93.1	6.6
17 α (H)-21 β (H)-hopane	127.0	7.7	125.2	8.2	111.1	7.1	649.8	57.2	184.6	13.8	124.9	9.5
<i>Steranes</i>												
$\alpha\beta\beta$ -20R-stigmastane	42.0	2.5	66.6	4.3	41.5	2.7	195.0	18.4	ND		ND	
$\alpha\beta\beta$ -20S-stigmastane ¹	37.9	2.3	47.8	3.1	29.5	1.9	155.4	15.2	ND		ND	
<i>PAHs</i>												
phenanthrene	19.9	2.8	105.2	10.7	27.8	5.0	61.5	12.6	125.4	13.9	235.6	22.4
anthracene	ND		ND		ND		ND		ND		79.2	9.8
A-methylphenanthrene	ND		110.1	24.4	20.4	23.2	ND		90.6	31.5	288.7	42.6
B-methylphenanthrene	ND		155.2	26.4	29.5	23.2	ND		191.0	35.4	364.9	46.9
C-methylphenanthrene	ND		65.9	23.1	11.7	23.1	ND		115.0	32.2	205.7	38.8
D-methylphenanthrene	ND		60.2	23.0	9.3	23.1	ND		90.5	31.5	148.4	36.8
fluoranthene	6.2	1.9	163.5	15.7	29.4	4.6	62.5	12.8	379.2	38.4	355.4	33.2
pyrene	10.1	3.0	361.1	34.2	74.5	9.1	200.8	26.1	950.8	95.5	559.2	52.0
benzo[ghi]fluoranthene	2.8	1.7	16.2	3.6	34.4	4.7	49.4	7.8	80.5	9.3	94.9	9.3
chrysene	2.3	2.2	ND		18.3	4.8	27.3	14.8	19.4	6.1	33.0	7.4
benzo[b]fluoranthene	5.5	6.1	ND		17.7	12.4	36.9	72.0	ND		51.9	33.2
benzo[k]fluoranthene	1.7	1.3	ND		ND		ND		ND		ND	
benzo[e]pyrene	5.6	2.5	ND		6.4	5.0	26.6	11.2	ND		ND	
benzo[a]pyrene	4.3	3.0	ND		5.8	5.9	ND		ND		ND	
indeno[1,2,3-cd]pyrene	2.4	5.7	ND		ND		ND		ND		ND	
benzo[ghi]perylene	12.4	3.4	ND		ND		ND		ND		ND	
coronene	ND		ND		ND		ND		ND		ND	

¹ Analyte identification based on comparisons to relative retention times to those in the literature.

² ND = not detected

Table 10. Ratio of analyte mass (μg) to organic carbon mass (g) for the MOUDI measurements for organic compounds emitted from HDDVs in the PM_{0.1} size fraction. Uncertainty values represent analytical uncertainty.

3.3.3 Comparison to Previous Measurements

The current study is the first to examine the size distribution of particulate trace organic species emitted from on-road heavy duty diesel vehicles operated under realistic dynamic driving cycles. Comparisons to previous measurements made using simpler test conditions can help to illustrate common trends in the data as well as emphasize new trends identified in the current tests due to the more realistic test conditions.

Zielinska, et al. [70] measured the size distribution of PAHs emitted from military diesel vehicles operated under steady-state load conditions. Most of the four to six ring nonvolatile PAHs detected in the current study were also observed in that previous work. Zielinska, et al. found that the emitted PAH size distribution was a function of engine load condition. Likewise, the results of the current study suggest that the peak in the PAH size distribution shifted to larger sizes for the idle-creep load condition vs. the full 5-mode HHDDT test.

Figure 11 shows a comparison of the emission factors ($\mu\text{g}/\text{km}$) measured in the current study with those of Rogge et. al. (1993) [13]. The top panel of Figure 11 shows that the emission rates of lubricating oil tracers measured in the current study are much lower (2-12 times) than those measured by Rogge. The oldest vehicle tested in the current study (1985 HDV) generally had the highest tracer emissions rates, suggesting that newer vehicles burn less lubricating oil. The center and bottom panel of Figure 11 compare emissions rates of light PAHs and heavy PAHs, respectively. The PAH emission rates for all vehicles examined in this study bracket those measured by Rogge. The PAH emissions rates for the 1992 Volvo and the 1985 Freightliner are two to four times higher than the emissions rate measured by Rogge, et al. For the newer vehicles, PAH emission rates were $\frac{2}{3}$ to $\frac{1}{2}$ of those reported by Rogge, et al. These results suggest that newer, lower mileage heavy duty trucks emit less PAHs per kilometer than older vehicles.

Figures 12 and 13 show that emission factors (μg analyte / kg of fuel burned) of three lubricating oil tracers measured in the current study fall in the range of values reported by other investigators in both the fine [13, 14, 70] and ultrafine (PM_{0.18}) [76] size fractions. Concentrations for heavy PAHs measured in this study also show strong agreement with previous measurements made using dilution systems [70] but were significantly lower than roadside measurements [76] for most analytes other than coronene in both the fine and ultrafine size fractions.

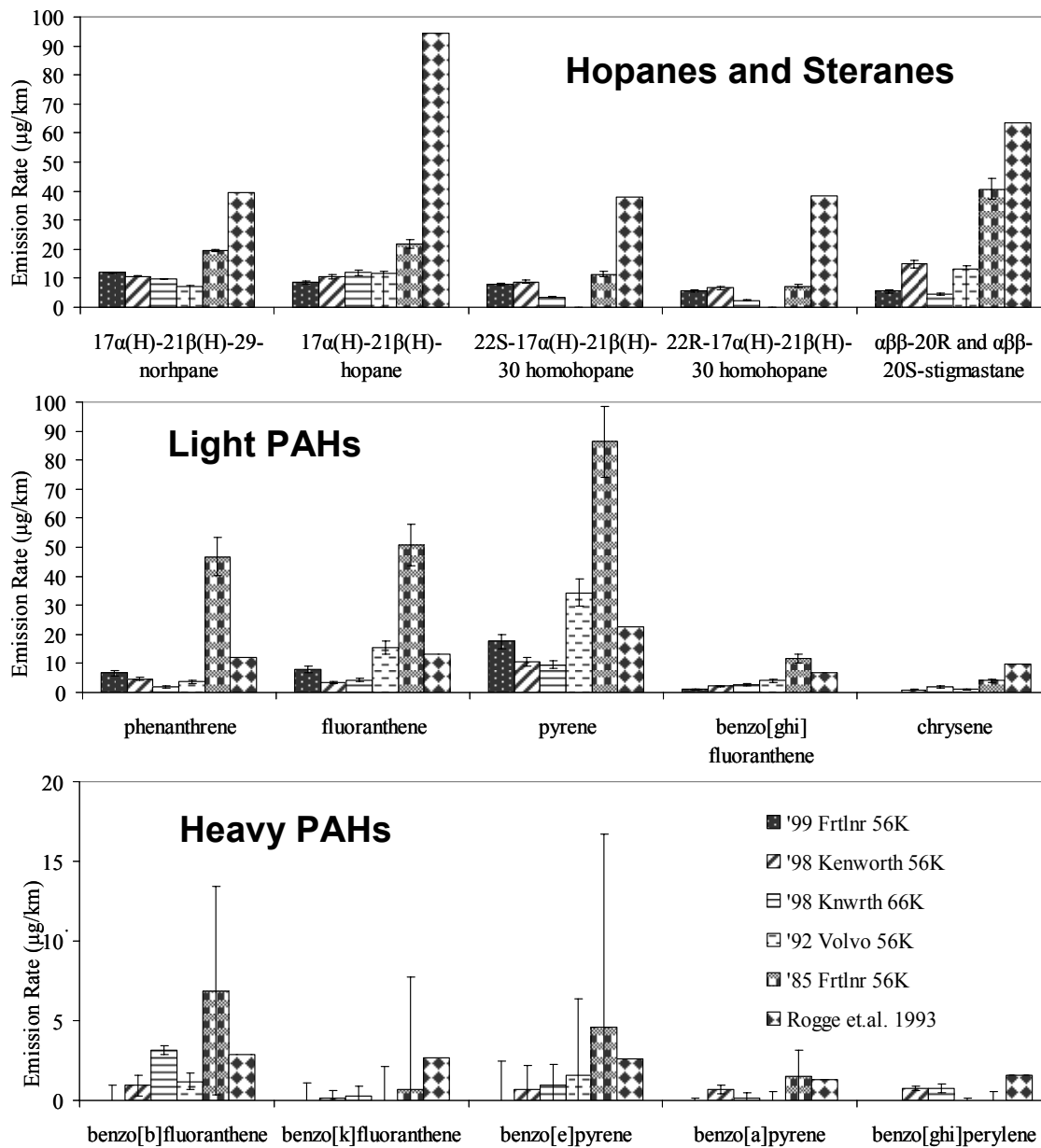


Figure 11. Comparison of PM 1.8 emission factors ($\mu\text{g}/\text{km}$) with those of Rogge, et al. 1993.

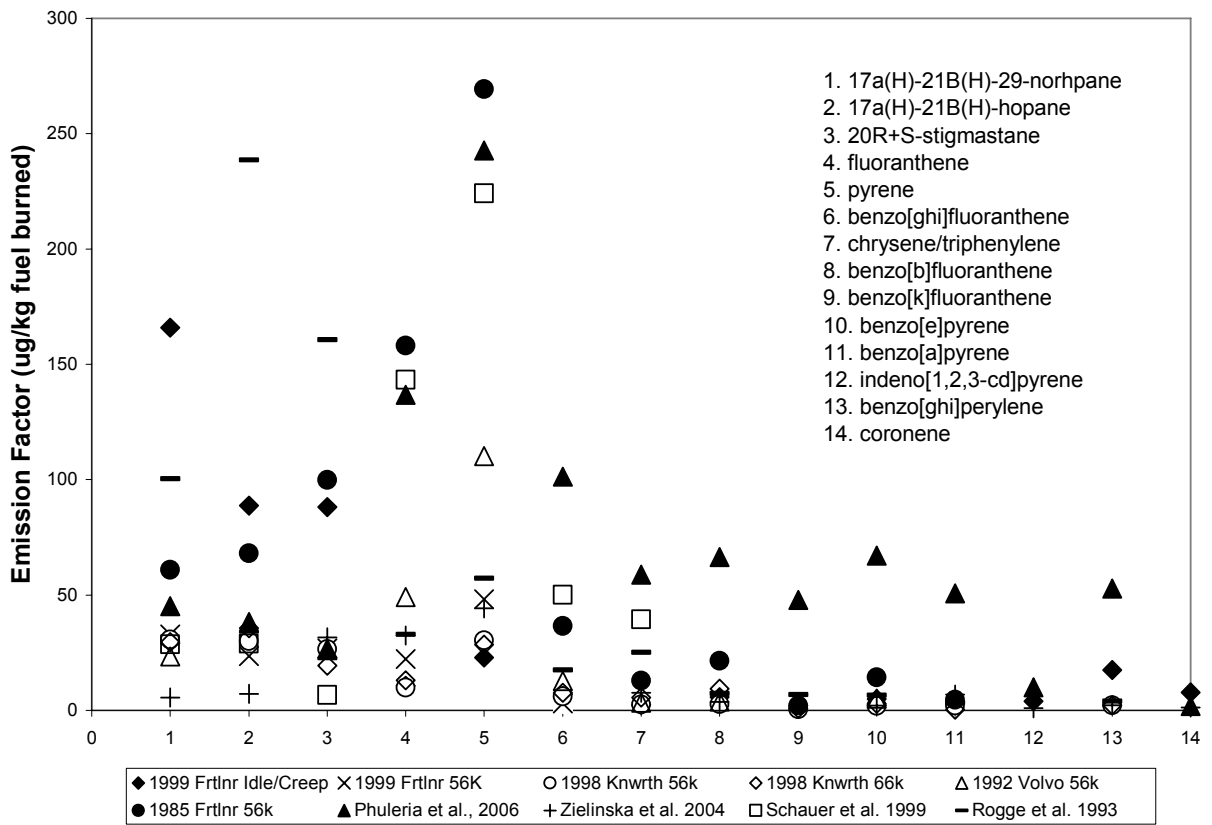


Figure 12: Comparison of PM1.8 emission factors (μg analyte / kg fuel burned) measured in the current study with those of Phuleria, et al. (2006), Zielinska, et al. (2004), Schauer, et al. (1999), and Rogge, et al. (1993).

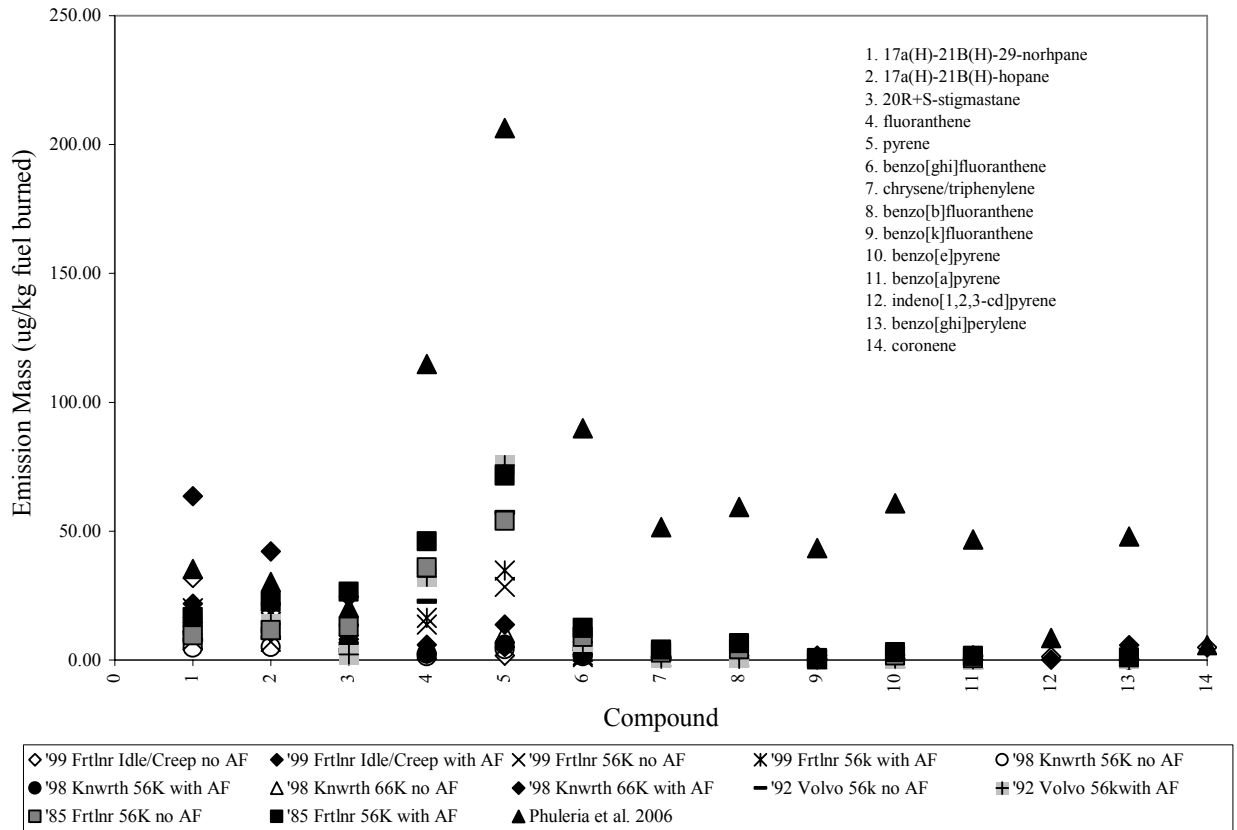


Figure 13: PM0.18 emissions factors measured in the current study with and without the MOUDI after filter (AF). Note that PM0.18 is not the definition of ultrafine particles used in the current study (PM0.1). Results measured by Phuleria, et al. 2006 are shown for comparison. PAH trends are similar to those shown in Figure 12.

3.4 Conclusions

Comparison between the mass of each trace organic compound collected by the MOUDI impactors and by the collocated filter samples shows a reasonable agreement for most analytes. All PAHs have size distributions that pass internal consistency QA/QC checks as shown in Table 8. Lubricating oil tracers 17 α (H)-21 β (H)-29-norhopane, 17 α (H)-21 β (H)-hopane, $\alpha\beta\beta$ -20R-stigmastane, and $\alpha\beta\beta$ -20S-stigmastane were identified as the four most self-consistent size-resolved PM emissions tracers. These tracers have approximately 10-20% of their mass in the ultrafine size fraction during both the idle+creep test and during the full 5-mode HHDDT cycle with 56,000 lbs inertial weight. This fraction increases to 20-45% for the higher load test with an inertial load of 66,000 lbs.

Noticeable trends in the size distributions are observed for both the lubricating oil tracers and the PAHs as a function of driving cycle. In the idle creep sample, both classes of compounds peak between 0.18-0.32 μm aerodynamic particle diameter. The PAH size distributions peak between 0.1-0.18 μm aerodynamic particle diameter for all 5-mode tests at either 56,000 lbs or 66,000 lbs. The hopane and sterane size distributions also peak between 0.080-0.143 during the 5-mode HHDDT test with 56,000 lbs inertial weight. The peak in the hopane and sterane size distributions shifts to 0.56 – 0.1 during the 66,000 lb inertial test.

Source profiles constructed using the relative abundance of trace organic compounds to total organic carbon mass are functions of vehicle age and load condition in both the fine and ultrafine size fractions. Increasing load conditions reduce the relative abundance of motor oil tracers in the PM1.8 size fraction but increase the relative abundance of these tracers in the PM0.1 size fraction. The relative abundances of PAHs in the PM0.1 and PM1.8 size fractions emitted from the oldest vehicle tested (1985 HDV) were significantly higher than for any other vehicle tested. The relative abundance of PAHs in the ultrafine size fraction is generally 2-3 times larger than in the PM1.8 size fraction. Tests with greater loads generally produced emissions with a greater relative abundance of light PAHs but with reduced concentrations of heavy PAHs. Some heavy PAHs were only observed during the idle and creep test.

4.0 METALS CONTENT OF DIESEL FUEL, MOTOR OIL, AND DIESEL PARTICULATE MATTER EMISSIONS

4.1 Introduction

The metals content of diesel fuel, motor oil, and fine PM emissions from each HDDV tested was determined using Inductively Coupled Plasma – Mass Spectrometry (ICP-MS) (7500i and 7500ce ICP-MS, Agilent Technologies, Inc., Palo Alto, CA). A method was developed using an Agilent 7500i ICP-MS to analyze the metals content of diesel fuel and motor oil; a separate method was developed using an Agilent 7500ce ICP-MS to analyze the metals content of bulk diesel PM emissions. These analyses indicate that the used motor oil contains the highest mass loading of metals, followed by the sampled tank fuel and lastly by the PM emissions. Size-resolved PM emissions metals distributions were not quantified because the projected concentrations fell below method detection limits.

4.2. Methodology

Two methods were developed and utilized in the analysis of HDDV-related metals. The first method was used to analyze the metals content of diesel fuel and motor oil taken from each HDDV. This method was run on an Agilent 7500i instrument with argon and oxygen as combustion gases – diesel fuel was run in its native form and motor oil was diluted in a certified oil-based ICP fluid (PremiSolv). The second method was used to analyze PM emissions from each HDDV as well as the diesel PM Standard Reference Material (SRM) 1650. This method was run on an Agilent 7500ce instrument with argon and oxygen as the combustion gases. Diesel PM collected from each HDDV on 47mm Teflon filters was first extracted in a solution of 75% acetone and 25% 1N HNO₃ – it was this matrix that was injected into the ICP-MS. An overview of each method is presented below in Table 11.

HDDV ICP-MS METHODOLOGY		
Metric	Fuel and Oil Samples	PM Emission Samples
Substrate Type	N/A	Teflon 47 mm
Instrument	Agilent 7500i	Agilent 7500ce
Extraction Matrix	N/A	30 mL 75/25 acetone/1N HNO ₃
Injection Matrix	5 mL PremiSolv ICP fluid, diesel fuel	30 mL 75/25 acetone/1N HNO ₃
Carrier Gas	argon	argon
Secondary Gas	oxygen	oxygen

Table 11. HDDV ICP-MS Methodology Summary

4.3 Results

4.3.1 ICP-MS Method Detection Limits

ICP-MS Method Detection Limits (MDLs) are shown for both methods in Table 12. MDLs were calculated in accordance with the U.S. E.P.A. protocol which defines an analytical MDL as three times the standard deviation of seven low concentration standards run over three non-consecutive days. MDLs for the fuel and oil sample method are higher than those than for the PM emission method – these methods differ in instrumentation as well as in their injection matrices and operational parameters. The higher MDLs in the fuel and oil methods are still well below the concentrations of many abundant metals detected in both diesel fuel and motor oil taken from the HDDVs tested.

HDDV ICP-MS MDLs (injection matrix concentrations)

Element (m/z)	fuel / oil		PM	
	(ug/L or ppb)			
Li / 7	52.3		0.696	
Na / 23	58.6		13.651	
Mg / 24			10.667	
Mg / 25	251.9		44.942	
Al / 27	65.2		35.928	
Si / 28				
Si / 29				
P / 31	137.8			
S / 34	202.5			
Cl / 35				
K / 39	228.7		7.088	
Ca / 40			11.888	
Ca / 43			28.422	
Sc / 45	56.0		39.814	
Ti / 47	73.0		44.565	
V / 51	15.0		0.056	
Cr / 52			1.183	
Cr / 53	149.3		4.195	
Mn / 55	78.6		0.045	
Fe / 57	18.9		7.861	
Co / 59	39.0		0.069	
Ni / 60	22.3		11.039	
Ni / 62	19.1		12.046	
Cu / 63	15.0		0.098	
Cu / 65	15.7		0.106	
Zn / 66	26.4		1.304	
Zn / 68	40.9		1.552	
Ga / 69	33.6		0.041	
Ga / 71	178.3		0.024	
Ge / 72			3.076	
As / 75	8.0		1.093	
Se / 77	16.3		5.567	
Se / 78			0.267	
Br / 79			1.370	
Rb / 85			0.064	
Sr / 88	62.2		0.038	
Y / 89	91.7		0.010	
Zr / 90	20.5		0.100	
Zr / 91	22.9		0.063	
Nb / 93			0.520	
Mo / 95	28.5		0.246	
Pd / 105	56.3		0.035	
Ag / 107	9.2		0.024	
Cd / 111	64.3		0.039	
Sn / 118	15.6		0.150	
Sb / 121	17.7		0.407	
Cs / 133			0.048	
Ba / 137	9.3		0.053	
La / 139	43.3		0.006	
Ce / 140			0.008	
Pr / 141			0.004	
Nd / 146			0.012	
Sm / 147			0.014	
Eu / 151			0.006	
Gd / 157			0.009	
Tb / 159				
Dy / 163			0.014	
Ho / 165			0.004	
Er / 166			0.010	
Tm / 169			0.007	
Yb / 172			0.011	
Lu / 175			0.011	
W / 182			2.796	
W / 183			24.497	
Pt / 195			49.573	
Tl / 205			0.483	
Pb / 208	22.0		0.809	
Bi / 209	65.7		0.472	
Th / 232			0.012	
U / 238			1.574	

Table 12. ICP-MS Method Detection Limits

4.3.2 Metals Analysis of Diesel SRM 1650

Diesel particulate matter Standard Reference Material (SRM) 1650 was generated from the heat exchangers of a dilution tube facility following 200 engine hours of particle accumulation from several direct injection four-cycle diesel engines operated under a variety of conditions. It is considered to be representative of heavy-duty diesel engine particulate emissions [77]. Although the metals content of SRM 1650 is not certified by NIST, Huggins, et al. used Particle Induced X-ray Emission (PIXE) to quantify the concentrations of 15 elemental components, presented below in Table 13. The results obtained via UCD's ICP-MS method agree very well with the data obtained by Huggins, et al. for 10 of the 14 elements that were common to each technique. The ICP-MS method detected three additional elements above MDL not detected by the PIXE method.

Element (m/z)	SRM 1650		
	Robert et al. ICP-MS	Huggins et al. PIXE	% diff (abs Δ / avg)
	ug/g	ppmm	%
Sodium / 23	0.1	< dl	
Magnesium / 25	46.9	< dl	
Aluminum / 27	61.7	< dl	
Silicon / 28	57.2	160	95%
Phosphorus / 31	662.3	740	11%
Sulfur / 34	53498.2	14500	115%
Chlorine / 35		120	
Potassium / 39	12.5	< dl	
Calcium / 40	2162.0	2300	6%
Titanium / 47	0.0	< dl	
Vanadium / 51	3.4	< dl	
Chromium / 52	70.3	62	13%
Manganese / 55	14.0	15	7%
Iron / 57	632.0	690	9%
Nickel / 60	66.8	50	29%
Copper / 63	56.6	50	12%
Zinc / 66	999.6	870	14%
Arsenic / 75	1.7	3.00	55%
Bromium / 79	7992.5	3.50	200%
Strontium / 88	5.7	< dl	
Cadmium / 111	6.2	< dl	
Lead / 208	31.3	23	30%

BOLD ITALICS indicates ICP-MS data that is below MDL

Table 13. ICP-MS vs. PIXE Analysis of Diesel PM SRM 1650

4.3.3. Metals Analyses of Diesel Fuel

Table 14 presents the ICP-MS metals analyses of diesel fuel sampled from each HDDV tested. Sodium, phosphorus, sulfur, iron, copper, zinc and lead were present above MDL in every sample. The fuel from HDDV 4 – the oldest vehicle tested – also contained significant amounts of magnesium with lesser amounts of titanium, manganese, nickel, gallium, strontium, silver, and tin. Since all of the fuel sampled was tank fuel, and assumed to be California reformulated diesel fuel, it is suspected that the additional metals loads from the older vehicles are entrained in the diesel fuel after it enters the vehicle.

Element (m/z)	Diesel Fuel			
	HDDV 1	HDDV 2	HDDV 3	HDDV 4
	ug / L	ug / L	ug / L	ug / L
Sodium / 23	787	761	3199	5198
Magnesium / 25	0	0	0	4580
Phosphorus / 31	2400	2325	4205	18839
Sulfur / 34	17089	17097	5153	14228
Titanium / 47	8	8	11	73
Manganese / 55	2	2	9	97
Iron / 57	51	50	220	3606
Nickel / 60	7	6	4	31
Copper / 63	51	51	39	1039
Copper / 65	49	48	38	996
Zinc / 66	178	181	11481	57979
Zinc / 68	156	151	10248	51212
Gallium / 69	0	0	23	140
Gallium / 71	346	0	152	1750
Strontium / 88	4	5	16	90
Molybdenum / 95	5	5	587	86
Silver / 107	6	7	2	24
Tin / 118	6	7	2	27
Barium / 137	0	1	39	214
Lead / 208	145	159	163	3474

BOLD ITALICS indicates ICP-MS data that is below MDL

Table 14. Results from ICP-MS Diesel Fuel Metals Analyses

4.3.4 Metals Analyses of Motor Oil

Table 15 presents the ICP-MS metals analyses of motor oil sampled from the three newest HDDVs tested; due to analytical instrumentation problems (clogging) data for the oldest vehicle is not reported. Many elements are above MDL at very significant concentrations – in excess of 1 gram per liter in the case of zinc for HDDV 2 and HDDV 3. Three of the most abundant metals detected – phosphorus, sulfur, and zinc – were also the most abundant metals detected in corresponding diesel fuel samples. This may indicate some cross-over metals contamination between the diesel fuel and motor oil within the diesel engine.

Element (m/z)	Motor Oil			
	HDDV 1	HDDV 2	HDDV 3	HDDV 4
	ug / L	ug / L	ug / L	ug / L
Lithium / 7	8	103	57	
Sodium / 23	451	116181	1741	
Magnesium / 25	30324	32257	41754	
Aluminum / 27	136	2525	781	
Phosphorus / 31	158024	478359	389576	
Sulfur / 34	34173	72943	68234	
Potassium / 39	0	120977	597	
Titanium / 47	664	1946	1490	
Vanadium / 51	7	29	13	
Chromium / 53	742	14286	491	
Manganese / 55	227	1594	195	
Iron / 57	16909	125275	15030	
Cobalt / 59	8	44	12	
Nickel / 60	76	351	153	
Nickel / 62	3	282	71	
Copper / 63	615	17418	1377	
Copper / 65	597	17318	1369	
Zinc / 66	637463	1220929	1098761	
Zinc / 68	563150	1088925	978266	
Gallium / 69	439	531	36	
Gallium / 71	18443	54728	39404	
Arsenic / 75	9	23	5	
Strontium / 88	311	1075	806	
Molybdenum / 95	35201	23362	59071	
Palladium / 105	40	332	110	
Silver / 107	12	228	116	
Cadmium / 111	24	278	113	
Tin / 118	93	2013	250	
Antimony / 121	6	137	11	
Barium / 137	602	693	55	
Lead / 208	735	41863	724	

BOLD ITALICS indicates ICP-MS data that is below MDL

Table 15. Results from ICP-MS Diesel Motor Oil Analyses

4.3.5 Metals Analyses of Diesel Exhaust PM

Table 16 presents the ICP-MS metals analyses of HDDV PM emissions sampled from all four HDDVs across the entire six test data set. Although the MDLs for this method are lower than those for the oil and fuel analyses method, the PM metals concentrations in diesel exhaust are also much lower – due to combustion and subsequent dilution – than those in either diesel fuel or motor oil. Since much of the data in Table 16 is near or below MDL, and these data represent bulk PM_{1.8} concentrations, MOUDI stage data were not analyzed as they would fall below MDLs.

All of the elements in Table 16 were detected in either the diesel fuel or motor oil samples discussed previously except for calcium. It is likely that calcium was present in the diesel fuel or motor oil but below the MDL for that method. Calcium has a mass to charge ratio of 40 and this is near the m/z of 44 for carbon dioxide, which is a by-product of carbon-to-oxygen bonding within the ICP-MS plasma. This interference is minimized in the PM analysis method by utilizing the Agilent 7500ce which incorporates a reaction cell to remove interfering molecules such as CO₂.

The mass of metal (ug) per mass of PM (g) for HDDV 1 and HDDV 2 is fairly consistent across the two tests for each vehicle, indicating that the metals composition of the PM is not strongly influenced by driving mode or inertial load on a mass-per-mass basis. However, this conclusion would not necessarily be true if the data were presented in different units such as ng/km or ng/liter of fuel consumed.

Element (m/z)	PM _{1.8} Emissions					
	HDDV 1		HDDV 2		HDDV 3	HDDV 4
	idle/creep	56k 5-mode	56k 5-mode	66k 5-mode	56k 5-mode	56k 5-mode
	ug / g	ug / g	ug / g	ug / g	ug / g	ug / g
Magnesium / 25	900.67	794.76	443.42	971.64	641.75	2128.02
Potassium / 39	4234.45	6006.66	7604.88	11001.86	3061.82	1996.94
Calcium / 40	2699.57	4373.06	3520.64	4987.51	5542.35	7495.91
Chromium / 53	164.29	383.25	612.14	490.82	219.87	73.04
Manganese / 55	35.93	48.29	95.27	123.37	37.84	31.47
Iron / 57	659.64	909.44	3490.99	1315.25	642.23	558.40
Copper / 63	68.12	248.04	143.62	416.16	73.45	148.02
Zinc / 66	3574.89	3869.39	2265.58	2103.86	2812.26	5244.13
Lead / 208	19.61	39.51	38.76	73.33	16.04	192.78

BOLD ITALICS indicates ICP-MS data that is below MDLs

Table 16. Results from ICP-MS Diesel PM Emissions Analyses

4.4 Conclusions

High mass loadings of 27 elements were quantified in motor oil samples from the HDDVs, and were dominated by phosphorus, sulfur, and zinc with lower concentrations of health-relevant metals such as cadmium, chromium, arsenic, strontium, and lead. Seventeen elements were detected in diesel fuel and at lower concentrations than in motor oil; phosphorus, sulfur, and zinc were also the most abundant metals detected. Up to nine metals were detected in PM emissions above MDL with potassium, calcium, and zinc present at significant concentrations. Sulfur was not observed in PM emissions; this can be attributed to low sulfur content California reformulated fuel as well as difficulty in measuring this metal using ICP-MS methodology.

5.0 CONCLUSIONS

Ultrafine and fine PM emissions were collected from four HDDVs using a chassis dynamometer and dilution source sampling system with a variety of sampling instrumentation. The four HDDVs were tested using the CARB HHDDT driving cycle and subjected to different inertial loads. Samples were analyzed for carbonaceous content, water soluble ions, trace organic species, and elemental composition. Real-time measurements were also reported.

Ultrafine and fine PM emissions were temporally correlated and increased with vehicle age for the full 5-mode HHDDT tests. However, the newest vehicle tested had the highest ultrafine PM mass emissions for the idle and creep test. The majority of both ultrafine and fine PM emissions were carbonaceous. The full 5-mode HHDDT tests were dominated by EC whereas the idle and creep test was dominated by OM. All PM size distributions peaked between 72 nm and 135 nm. Calcium was the most abundant water-soluble ion identified in the PM samples.

$17\alpha(H)$ - $21\beta(H)$ -29-norhopane, $17\alpha(H)$ - $21\beta(H)$ -hopane, $\alpha\beta\beta$ -20R-stigmastane, and $\alpha\beta\beta$ -20S-stigmastane were identified as the four most useful size-resolved PM emissions tracers. The size distribution of these compounds all peak between 0.143-0.253 μm aerodynamic particle diameter of the idle and creep test, between 0.080-0.143 μm aerodynamic particle diameter for all 56,000 lb inertial load 5-mode tests, and between 0.040 – 0.080 μm for the 66,000 lb inertial load 5-mode test. The ratio of ultrafine PM to total OM is highest for the 66,000 lb inertial load and lowest for the idle and creep test. No consistent trend in the percentage of OC was observed for the remaining 56,000 lb tests. All PAHs have size distributions that pass internal consistency QA/QC checks. PAHs peak between 0.080-0.143 μm aerodynamic particle diameter for the idle and creep test and between 0.080-0.143 μm aerodynamic particle diameter for all 56,000 lb and 66,000 lb tests.

High mass loadings of 27 elements were quantified in motor oil samples from the HDDVs. The most abundant elements were phosphorus, sulfur, and zinc with lower concentrations of health-relevant metals such as cadmium, chromium, arsenic, strontium, and lead. Seventeen elements were detected in diesel fuel at lower concentrations than in motor oil including phosphorus, sulfur, and zinc. Up to nine metals were detected in PM emissions above MDL with potassium, calcium, and zinc present at the highest concentrations. Sulfur was not observed in PM emissions; this can be attributed to low sulfur content California reformulated fuel as well as difficulty in measuring this metal using ICP-MS methodology.

6.0 REFERENCES

1. Levy, J.I., J.K. Hammitt, and J.D. Spengler, *Estimating the mortality impacts of particulate matter: What can be learned from between-study variability?* Environmental Health Perspectives, 2000. **108**(2): p. 109-117.
2. Dockery, D.W., C.A. Pope, 3rd, X. Xu, J.D. Spengler, J.H. Ware, M.E. Fay, B.G. Ferris, Jr., and F.E. Speizer, *An association between air pollution and mortality in six U.S. cities.* New England journal of medicine, 1993. **329**(24): p. 1753-9.
3. Samet, J.M., F. Dominici, F.C. Curriero, I. Coursac, and S.L. Zeger, *Fine particulate air pollution and mortality in 20 US Cities, 1987-1994.* New England Journal of Medicine, 2000. **343**(24): p. 1742-1749.
4. Venkataraman, C. and A.S. Kao, *Comparison of particle lung doses from the fine and coarse fractions of urban PM-10 aerosols.* Inhalation Toxicology, 1999. **11**(2): p. 151-169.
5. Oberdorster, G., R.M. Gelein, J. Ferin, and B. Weiss, *Association of Particulate Air-Pollution and Acute Mortality - Involvement of Ultrafine Particles.* Inhalation Toxicology, 1995. **7**(1): p. 111-124.
6. Schwartz, J. and L.M. Neas, *Fine particles are more strongly associated than coarse particles with acute respiratory health effects in schoolchildren.* Epidemiology, 2000. **11**(1): p. 6-10.
7. Penttinen, P., K.L. Timonen, P. Tiittanen, A. Mirme, J. Ruuskanen, and J. Pekkanen, *Ultrafine particles in urban air and respiratory health among adult asthmatics.* European Respiratory Journal, 2001. **17**(3): p. 428-435.
8. Peters, A., H.E. Wichmann, T. Tuch, J. Heinrich, and J. Heyder, *Respiratory effects are associated with the number of ultrafine particles.* American Journal Of Respiratory And Critical Care Medicine, 1997. **155**(4): p. 1376-1383.
9. Wichmann, H.E.S., C.; Tuch, T.; Wolke, G.; Peters, A.; Heinrich, J.; Kreyling, G.; Heyder, J. , *Daily mortality and fine and ultrafine particles in Erfurt, Germany, Part I: Role of particle number and particle mass.* Health Effects Institute Research Report 98, 2000.
10. Li, N., C. Sioutas, A. Cho, D. Schmitz, C. Misra, J. Sempf, M.Y. Wang, T. Oberley, J. Froines, and A. Nel, *Ultrafine particulate pollutants induce oxidative stress and mitochondrial damage.* Environmental Health Perspectives, 2003. **111**(4): p. 455-460.
11. Lloyd, A.C. and T.A. Cackette, *Diesel engines: Environmental impact and control.* Journal of the Air & Waste Management Association, 2001. **51**(6): p. 809-847.
12. Hildemann, L.M., G.R. Markowski, and G.R. Cass, *Chemical composition of emissions from urban sources of fine organic aerosol.* Environmental Science and Technology, 1991. **25**(4): p. 744-59.
13. Rogge, W.F., L.M. Hildemann, M.A. Mazurek, G.R. Cass, and B.R.T. Simoneit, *Sources of fine organic aerosol. 2. Noncatalyst and catalyst-equipped automobiles and heavy-duty diesel trucks.* Environmental Science and Technology, 1993. **27**(4): p. 636-51.

14. Schauer, J.J., M.J. Kleeman, G.R. Cass, and B.R.T. Simoneit, *Measurement of emissions from air pollution sources. 2. C-1 through C-30 organic compounds from medium duty diesel trucks*. Environmental Science & Technology, 1999. **33**(10): p. 1578-1587.
15. Lowenthal, D.H., B. Zielinska, J.C. Chow, J.G. Watson, M. Gautam, D.H. Ferguson, G.R. Neuroth, and K.D. Stevens, *Characterization of Heavy-Duty Diesel Vehicle Emissions*. Atmospheric Environment, 1994. **28**(4): p. 731-743.
16. Shi, J.P., D. Mark, and R.M. Harrison, *Characterization of particles from a current technology heavy-duty diesel engine*. Environmental Science & Technology, 2000. **34**(5): p. 748-755.
17. (CalEPA), C.E.P.A., *Proposed Identification of Diesel Exhaust as a Toxic Air Contaminant*. 1998, Prepared by the Air Resources Board and Office of Environmental Health Hazard Assessment.
18. EPA, U.S., *Code of Federal Regulations 40 CFR Part 80*. 2001. p. 17230-17273.
19. Schauer, J.J., W.F. Rogge, L.M. Hildemann, M.A. Mazurek, G.R. Cass, and B.R.T. Simoneit, *Source apportionment of airborne particulate matter using organic compounds as tracers*. Atmospheric Environment, 1996. **30**(22): p. 3837-3855.
20. (USEPA), U.S.E.P.A., *Health Assessment Document for Diesel Engine Exhaust*. 2002, Prepared by the National Center for Environmental Assessment for the Office of Transportation and Air Quality.
21. Eldering, A. and G.R. Cass, *Source-oriented model for air pollutant effects on visibility*. Journal of Geophysical Research-Atmospheres, 1996. **101**(D14): p. 19343-19369.
22. Ackerman, A.S., O.B. Toon, J.P. Taylor, D.W. Johnson, P.V. Hobbs, and R.J. Ferek, *Effects of aerosols on cloud albedo: Evaluation of Twomey's parameterization of cloud susceptibility using measurements of ship tracks*. Journal of the Atmospheric Sciences, 2000. **57**(16): p. 2684-2695.
23. EPA, U.S., *Regulatory Announcement EPA420-F-00-055*. 2000.
24. Saitoh, K., K. Sera, T. Shirai, T. Sato, and M. Odaka, *Determination of elemental and ionic compositions for diesel exhaust particles by particle induced X-ray emission and ion chromatography analysis*. Analytical Sciences, 2003. **19**(4): p. 525-528.
25. Holmen, B.A. and A. Ayala, *Ultrafine PM emissions from natural gas, oxidation-catalyst diesel, and particle-trap diesel heavy-duty transit buses*. Environmental Science & Technology, 2002. **36**(23): p. 5041-5050.
26. Hildemann, L.M., G.R. Markowski, M.C. Jones, and G.R. Cass, *Submicrometer aerosol mass distributions of emissions from boilers, fireplaces, automobiles, diesel trucks, and meat-cooking operations*. Aerosol Science and Technology, 1991. **14**(1): p. 138-52.
27. Zanini, G., M. Berico, F. Monforti, L. Vitali, S. Zambonelli, S. Chiavarini, T. Georgiadis, and M. Nardino, *Concentration measurement in a road tunnel as a method to assess "real-world" vehicles exhaust emissions*. Atmospheric Environment, 2006. **40**(7): p. 1242-1254.

28. Miguel, A.H., T.W. Kirchstetter, R.A. Harley, and S.V. Hering, *On-road emissions of particulate polycyclic aromatic hydrocarbons and black carbon from gasoline and diesel vehicles*. Environmental Science & Technology, 1998. **32**(4): p. 450-455.
29. Geller, V.D., S.B. Sardar, H. Phuleria, P.N. Fine, and C. Sioutas, *Measurements of particle number and mass concentrations and size distributions in a tunnel environment*. Environmental Science & Technology, 2005. **39**(22): p. 8653-8663.
30. He, L.Y., M. Hu, Y.H. Zhang, B.D. Yu, and D.Q. Liu, *Chemical characterization of fine particles from on-road vehicles in the Wutong tunnel in Shenzhen, China*. Chemosphere, 2006. **62**(10): p. 1565-1573.
31. Park, K., F. Cao, D.B. Kittelson, and P.H. McMurry, *Relationship between particle mass and mobility for diesel exhaust particles*. Environmental Science & Technology, 2003. **37**(3): p. 577-583.
32. Sharma, M., A.K. Agarwal, and K.V.L. Bharathi, *Characterization of exhaust particulates from diesel engine*. Atmospheric Environment, 2005. **39**(17): p. 3023-3028.
33. Gross, D.S., M.E. Galli, P.J. Silva, S.H. Wood, D.-Y. Liu, and K.A. Prather, *Single particle characterization of automobile and diesel truck emissions in the Caldecott Tunnel*. Aerosol Science and Technology, 2000. **32**(2): p. 152-163.
34. Suess, D.T. and K.A. Prather, *Reproducibility of single particle chemical composition during a heavy duty diesel truck dynamometer study*. Aerosol Science and Technology, 2002. **36**(12): p. 1139-1141.
35. Hildemann, L.M., G.R. Cass, and G.R. Markowski, *A Dilution Stack Sampler for Collection of Organic Aerosol Emissions: Design, Characterization and Field Tests*. Aerosol Science and Technology, 1989. **10**: p. 193-204.
36. Shah, S.D., D.R. Cocker, J.W. Miller, and J.M. Norbeck, *Emission rates of particulate matter and elemental and organic carbon from in-use diesel engines*. Environmental Science & Technology, 2004. **38**(9): p. 2544-2550.
37. Molodano, H., *California Air Resources Board, Sacramento, CA*. 2004.
38. Robert, M.A., C.A. Jakober, and M.J. Kleeman, *Size and Composition Distribution of Particulate Matter 1. Light-duty Gasoline Vehicles*. Journal of the Air and Waste Management Association, in review 2006.
39. NIOSH, *NIOSH Manual of Analytical Methods, 4th ed. (1st Supplement)*. 1996, National Institute for Occupational Safety and Health: Cincinnati, OH.
40. Birch, M.E. and R.A. Cary, *Elemental carbon-based method for monitoring occupational exposures to particulate diesel exhaust*. Aerosol Science and Technology, 1996. **25**(3): p. 221-241.
41. Gray, H.A., G.R. Cass, J.J. Huntzicker, E.K. Heyerdahl, and J.A. Rau, *Elemental and Organic-Carbon Particle Concentrations - a Long-Term Perspective*. Science of the Total Environment, 1984. **36**(JUN): p. 17-25.
42. Chung, A., J.D. Herner, and M.J. Kleeman, *Detection of alkaline ultrafine atmospheric particles at Bakersfield, California*. Environmental Science & Technology, 2001. **V35 N11**(JUN 1): p. 2184-2190.

43. Bukowiecki, N., D.B. Kittelson, W.F. Watts, H. Burtscher, E. Weingartner, and U. Baltensperger, *Real-time characterization of ultrafine and accumulation mode particles in ambient combustion aerosols*. Journal of Aerosol Science, 2002. **33**(8): p. 1139-1154.
44. Cocker, D.R., S.D. Shah, K. Johnson, J.W. Miller, and J.M. Norbeck, *Development and application of a mobile laboratory for measuring emissions from diesel engines. 1. Regulated gaseous emissions*. Environmental Science & Technology, 2004. **38**(7): p. 2182-2189.
45. Toner, S.M., D.A. Sodeman, and K.A. Prather, *Single particle characterization of ultrafine and accumulation mode particles from heavy duty diesel vehicles using aerosol time-of-flight mass spectrometry*. Environmental Science & Technology, 2006. **40**(12): p. 3912-3921.
46. Fraser, M.P., K. Lakshmanan, S.G. Fritz, and B. Ubanwa, *Variation in composition of fine particulate emissions from heavy-duty diesel vehicles*. Journal of Geophysical Research, [Atmospheres], 2002. **107**(D21): p. ICC8/1-ICC8/6.
47. Larson, S.M., G.R. Cass, K.J. Hussey, and F. Luce, *Verification of Image-Processing Based Visibility Models*. Environmental Science & Technology, 1988. **22**(6): p. 629-637.
48. Park, K., D.B. Kittelson, and P.H. McMurry, *Structural properties of diesel exhaust particles measured by transmission electron microscopy (TEM): Relationships to particle mass and mobility*. Aerosol Science And Technology, 2004. **38**(9): p. 881-889.
49. Kasper, G., *Dynamics And Measurement Of Smokes .1. Size Characterization Of Non-Spherical Particles*. Aerosol Science And Technology, 1982. **1**(2): p. 187-199.
50. Ahlvik, P.N., Leonidas; Keskinen, Jorma; Virtanen, Anelle, *Real Time Measurements of Diesel Particle Size Distribution with an Electrical Low Pressure Impactor*. SAE Technical Paper Series, 1998(980410).
51. Maricq, M.M., D.H. Podsiadlik, and R.E. Chase, *Size distributions of motor vehicle exhaust PM: A comparison between ELPI and SMPS measurements*. Aerosol Science And Technology, 2000. **33**(3): p. 239-260.
52. Virtanen, A.R., Jyrki; Marjamäki, Marko; Vaaraslahti, Kati; Keskinen. Jorma; Lappi; Maiji, *Effective Density of Diesel Exhaust Particles as a Function of Size*. SAE Technical Paper Series, 2002(2002-01-0056).
53. McMurry, P.H., X. Wang, K. Park, and K. Ehara, *The relationship between mass and mobility for atmospheric particles: A new technique for measuring particle density*. Aerosol Science And Technology, 2002. **36**(2): p. 227-238.
54. (USDOE), U.S.D.o.E., *Documentation for Emissions of Greenhouse Gases in the United States 2002*. 2004, Office of Integrated Analysis and Forecasting, U.S. Department of Energy: Washington D.C.
55. Kleeman, M.J., J.J. Schauer, and G.R. Cass, *Size and Composition Distribution of Fine Particulate Matter Emitted from Motor Vehicles*. Environmental Science and Technology, 2000. **34**(7): p. 1132-1142.
56. Bagley, S.T., *Characterization of Fuel and Aftertreatment Device Effects on Diesel Emissions*. Health Effects Institute Technical Report 76, 1996.

57. Erkki, L.P.M.J., Ojanen; Kati, Vaaraslahti; Jorma, Keskinen, *Sampling and Engine After-Treatment Effect On Diesel Exhaust Particle Size Distributions*. SAE Technical Paper Series, 2005(2005-01-0192).
58. Schauer, J.J., W.F. Rogge, L.M. Hildemann, M.A. Mazurek, and G.R. Cass, *Source apportionment of airborne particulate matter using organic compounds as tracers*. Atmospheric Environment, 1996. **30**(22): p. 3837-3855.
59. Gertler, A.W., J.A. Gillies, and W.R. Pierson, *An assessment of the mobile source contribution to PM10 and PM2.5 in the United States*. Water, Air, and Soil Pollution, 2000. **123**(1-4): p. 203-214.
60. Fraser, M.P., Z.W. Yue, and B. Buzcu, *Source apportionment of fine particulate matter in Houston, TX, using organic molecular markers*. Atmospheric Environment, 2003. **37**(15): p. 2117-2123.
61. Kleeman, M.J. and G.R. Cass, *Source contributions to the size and composition distribution of urban particulate air pollution*. Atmospheric Environment, 1998. **32**(16): p. 2803-2816.
62. Cass, G.R., L.A. Hughes, P. Bhave, M.J. Kleeman, J.O. Allen, and L.G. Salmon, *The chemical composition of atmospheric ultrafine particles*. Philosophical Transactions of the Royal Society of London Series A-Mathematical Physical and Engineering Sciences, 2000. **V358 N1775**(OCT 15): p. 2581-2592.
63. Daigle, C.C., D.C. Chalupa, F.R. Gibb, P.E. Morrow, G. Oberdorster, M.J. Utell, and M.W. Frampton, *Ultrafine particle deposition in humans during rest and exercise*. Inhalation Toxicology, 2003. **15**(6): p. 539-552.
64. Ibald-Mulli, A., H.E. Wichmann, W. Kreyling, and A. Peters, *Epidemiological evidence on health effects of ultrafine particles*. Journal of Aerosol Medicine-Deposition Clearance and Effects in the Lung, 2002. **15**(2): p. 189-201.
65. Tsai, F.C., M.G. Apte, and J.M. Daisey, *An exploratory analysis of the relationship between mortality and the chemical composition of airborne particulate matter*. Inhalation Toxicology, 2000. **12**(Suppl. 2): p. 121-135.
66. Adonis, M.I., R.M. Riquelme, V.D. Martinez, L. Gil, C. Rios, L. Rodriguez, and E.M. Rodriguez, *PAHs and Mutagenicity of Inhalable and Respirable Diesel Particulate Matter in Santiago, Chile*. Polycyclic Aromatic Compounds, 2003. **23**(5): p. 495-514.
67. Bostrom, E., S. Engen, and I. Eide, *Mutagenicity testing of organic extracts of diesel exhaust particles after spiking with polycyclic aromatic hydrocarbons (PAH)*. Archives of Toxicology, 1998. **72**(10): p. 645-649.
68. Flowers, L., S.H. Rieth, V.J. Cogliano, G.L. Foureman, R. Hertzberg, E.L. Hofmann, D.L. Murphy, S. Nesnow, and R.S. Schoeny, *Health assessment of polycyclic aromatic hydrocarbon mixtures: current practices and future directions*. Polycyclic Aromatic Compounds, 2002. **22**(3-4): p. 811-821.
69. Rogge, W.F., L.M. Hildemann, M.A. Mazurek, G.R. Cass, and B.R.T. Simoneit, *Mathematical modeling of atmospheric fine particle-associated primary organic compound concentrations*. Journal of Geophysical Research, 1996. **101**(D14): p. 19379-19394.

70. Zielinska, B., J.C. Sagebiel, W.P. Arnott, C.F. Rogers, K.E. Kelly, D.A. Wagner, J.S. Lighty, A.F. Sarofim, and G. Palmer, *Phase and Size Distribution of Polycyclic Aromatic Hydrocarbons in Diesel and Gasoline Vehicle Emissions*. Environmental Science & Technology, 2004. **38**: p. 2557-2567.
71. Chow, J.C., *Diesel engines: Environmental impact and control*. Journal of the Air & Waste Management Association, 2001. **51**(9): p. 1258-1270.
72. Watson, J.G., J.C. Chow, and J.E. Houck, *PM_{2.5} chemical source profiles for vehicle exhaust, vegetative burning, geological material, and coal burning in Northwestern Colorado during 1995*. Chemosphere, 2001. **43**(8): p. 1141-1151.
73. Robert, M.A., C.A. Jakober, S. VanBergen, and M.J. Kleeman, *Size and Composition Distribution of Particulate Matter 2. Heavy-duty Diesel Vehicles*. Journal of the Air and Waste Management Association, *in review* 2006.
74. Cass, G.R., *Organic molecular tracers for particulate air pollution sources*. TrAC, Trends in Analytical Chemistry, 1998. **17**(6): p. 356-366.
75. Kweon, C.-B., S. Okada, D.E. Foster, M.-S. Bae, and J.J. Schauer, *Effect of engine operating conditions on particle-phase organic compounds in engine exhaust of a heavy-duty direct-injection (D.I.) diesel engine*. Society of Automotive Engineers, [Special Publication] SP, 2003. **SP-1738**(In-Cylinder Diesel Particulate and NO_x Control 2003): p. 73-89.
76. Phuleria, H.C., M.D. Geller, P.M. Fine, and C. Sioutas, *Size-resolved emissions of organic tracers from light- and heavy-duty vehicles measured in a California roadway tunnel*. Environmental Science and Technology, 2006. **40**: p. 4109-4118.
77. Huggins, F.E., G.P. Huffman, and J.D. Robertson, *Speciation of elements in NIST particulate matter SRMs 1648 and 1650*. Journal Of Hazardous Materials, 2000. **74**(1-2): p. 1-23.